Research Square

Preprints are preliminary reports that have not undergone peer review.
They should not be considered conclusive, used to inform clinical practice,
or referenced by the media as validated information.

Pillar Chemistry Controls Adsorption Pathways in Bentonite: Mechanistic Insights into Efficient Ampicillin Removal from Hospital Wastewater

Prashant Pandey

prashant.pandey@upwr.edu.pl

Wroclaw University of Environmental and Life Sciences

Manisha Dhiman

Chandigarh University

Amit Pokhriyal

Uttarakhand Pollution Control Board- Dehradun- 248001

Chinenye Adaobi Igwegbe

Wroclaw University of Environmental and Life Sciences

Andrzej Białowiec

Wroclaw University of Environmental and Life Sciences

Lukasz Bobak

Wroclaw University of Environmental and Life Sciences

Article

Keywords: Clay, Medicinal, Hybrid microwave-sonochemical, Process intensification, Wastewater treatment, Sustainable adsorbents

Posted Date: August 4th, 2026

DOI: https://doi.org/10.21203/rs.3.rs-10402650/v1

License: This work is licensed under a Creative Commons Attribution 4.0 International License.
Read Full License

Additional Declarations: No competing interests reported.

Pillar Chemistry Controls Adsorption Pathways in Bentonite: Mechanistic Insights into Efficient Ampicillin Removal from Hospital Wastewater

Prashant Pandey[1*], Manisha Dhiman[2], Amit Pokhriyal[3], Chinenye Adaobi Igwegbe[1,4], Andrzej Białowiec[5,] Lukasz Bobak[6]

[1]Department of Applied Bioeconomy, Wroclaw University of Environmental and Life Sciences, 51-630 Wrocław, Poland,
[2]Institute of Liberal Arts and Humanities (Economics), Chandigarh University, Mohali, Punjab, India
[3]Uttarakhand Pollution Control Board- Dehradun- 248001, Uttarakhand, India
[4]Department of Chemical Engineering, Nnamdi Azikiwe University, P.M.B. 5025, Awka 420218, Nigeria,
[5]Łukasiewicz Research Network - PORT Polish Centre for Technology Development, Stablowicka 147 Str., 54-066Wroclaw, Poland
[6]Department of Functional Food Product Development, Wroclaw University of Environmental and Life Sciences, 51-630 Wrocław, Poland.

*Corresponding author's email address: Prashant Pandey; prashant.pandey@upwr.edu.pl

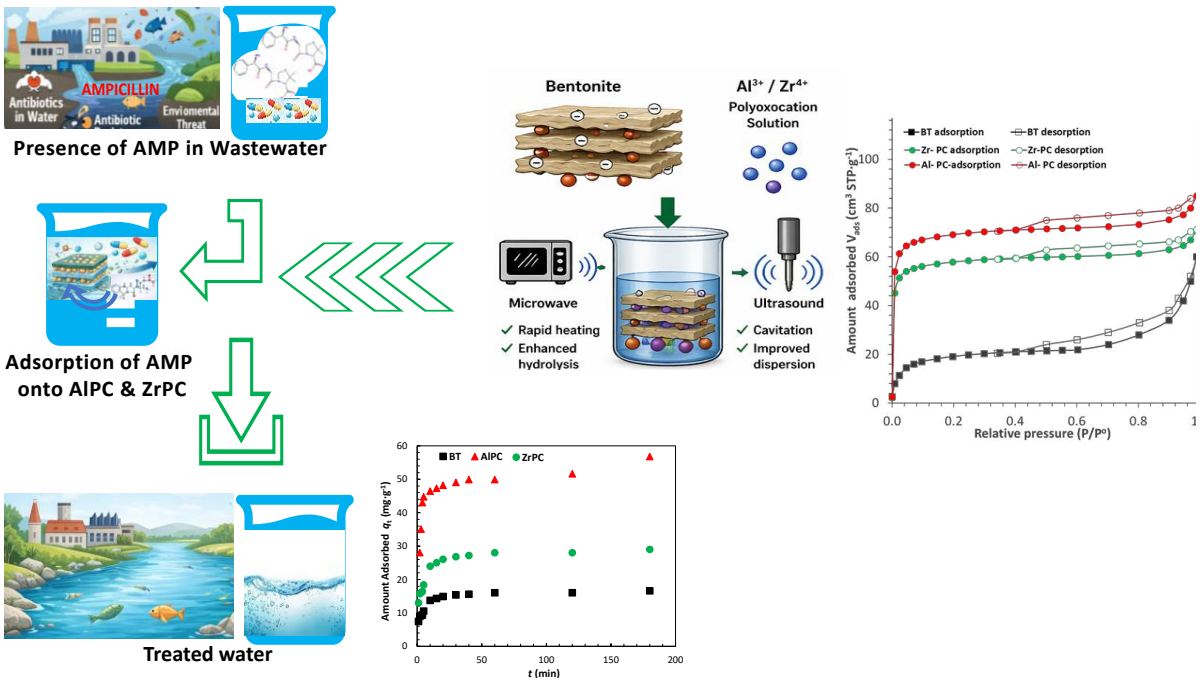
Abstract

β-Lactam antibiotics in aquatic environments pose significant environmental and public health risks owing to their persistence and contribution to antimicrobial resistance. However, the influence of pillar chemistry and synthesis strategy on the structure-performance relationship of pillared clays remains insufficiently understood. In the present study, aluminium- and zirconium-pillared bentonite were synthesized using a microwave-sonochemical hybrid approach that was designed to promote controlled hydrolysis, intercalation, and dispersion of metal polycations within the clay framework. The structural modification increased the specific surface area from 53 to 272 $m^2 . g^{-1}$ and significantly enhanced the adsorption performance toward ampicillin. Equilibrium data were satisfactorily described by the Langmuir isotherm, while adsorption kinetics followed the pseudo-second-order model. The maximum adsorption capacities at 298 K were 73.67 mg. g^{-1} for AlPC, 59.17 mg. g^{-1} for ZrPC, and 16.17 mg. g^{-1} for pristine bentonite. The developed adsorbents were further validated using a representative hospital wastewater matrix obtained from Doon Hospital effluents. Mechanistic analyses

suggest that adsorption involves electrostatic interactions, hydrogen bonding, Lewis acid-base interactions, and pore-filling effects within the expanded interlayer structure. The materials retained satisfactory adsorption performance over three adsorption-desorption cycles using NaOH. A preliminary laboratory-scale cost assessment suggests potential economic viability that requires further validation.

Keywords: Clay, Medicinal, Hybrid microwave-sonochemical, Process intensification, Wastewater treatment, Sustainable adsorbents.

Graphical abstract



1. Introduction

Antibiotics play a vital role in suppressing the growth and proliferation of pathogenic microorganisms, including bacteria, protozoa, and fungi. Consequently, they are extensively employed not only in human medicine but also across livestock farming, veterinary practice, poultry production, and agriculture to prevent and treat infectious diseases [1,2]. The global

consumption of antibiotics has therefore increased steadily over recent decades, driven by rising healthcare demands and intensified agricultural practices. However, a significant fraction of administered antibiotics is not fully metabolised within the body; instead, unmetabolized parent compounds and active metabolites are excreted and subsequently enter wastewater streams. This continuous release has led to the classification of antibiotics as emerging environmental contaminants of growing concern [3].

Among antibiotic classes, β-lactam antibiotics are among the most widely consumed worldwide, resulting in their persistent discharge into aquatic environments. Ampicillin (AMP), a broad-spectrum β-lactam antibiotic, has been repeatedly detected in sewage systems and wastewater effluents at concentrations ranging from ng. L^{-1} to μg. L^{-1} [4,5]. This antibiotic is commonly prescribed for the treatment of severe bacterial infections, including meningitis, respiratory tract infections, gastrointestinal disorders, urinary tract infections, and infections of the reproductive system [6–8]. Due to its extensive medical use and incomplete removal during wastewater treatment, AMP has become one of the most frequently detected antibiotics in environmental matrices.

The environmental persistence of antibiotics represents a critical challenge, particularly in the context of antimicrobial resistance (AMR). The World Health Organisation (WHO) has identified approximately 260 medicines as critically important for human health, many of which are antibiotics. After their intended use, these compounds are directly or indirectly released into surface water, groundwater, drinking water sources, and soil environments [9–11]. Continuous exposure of microorganisms to sub-lethal concentrations of antibiotics can accelerate the proliferation of antibiotic-resistant bacteria and resistance genes, thereby compromising the effectiveness of existing therapies and posing a substantial threat to public health [12].

Several studies have reported the persistence of AMP in sewage treatment plant (STP) effluents, even after conventional biological treatment. For example, Kulkarni et al. (2017) observed measurable concentrations of antibiotics in reclaimed water used for spray irrigation in the United States, despite the application of ultraviolet disinfection, with concentrations reaching tens of ng. mL^{-1} depending on the antibiotic type. These findings highlight the limited efficiency of conventional treatment processes in eliminating pharmaceutical residues and emphasise the urgent need for advanced treatment strategies capable of removing antibiotics from wastewater.

Among various treatment technologies (such as hydrolysis, photolysis, biodegradation, and oxidation-reduction), adsorption is recognised as a particularly attractive approach for trace organic removal due to its simplicity, flexibility, and cost-effectiveness. The adsorption technique offers simple operation, no need for complex equipment, and ease of large-scale application, with wide availability of adsorbents, including those derived from agricultural wastes and industrial residues, resulting in low costs and high removal efficiency even for low-concentration antibiotics [14–17]. A wide range of adsorbents has been explored, including activated carbons, porous polymers, graphene-based materials, and magnetic nanocomposites. Carbon- and silica-based materials are particularly attractive owing to their chemical stability, resistance to acidic and alkaline environments, and high adsorption capacity. [18] demonstrated effective AMP removal using rice husk - derived adsorbents. However, many high-performance adsorbents rely on chemical activation or complex synthesis routes, which can increase operational costs and introduce secondary pollution concerns.

In this context, natural clay minerals such as bentonite (BT) have gained increasing attention as low-cost, abundant, and environmentally benign adsorbents. Bentonite possesses a high cation-exchange capacity and a layered swelling structure, which is capable of holding

contaminant molecules. However, pristine bentonite typically exhibits limited adsorption capacity for organic micropollutants due to its relatively low surface area and insufficient active sites. To address these limitations, surface modification strategies including ion exchange, intercalation, and pillaring have been developed to enhance the adsorption performance of bentonite. Modified Ponorogo bentonite was explored for the adsorptive removal of AMP [19]. Many studies have investigated the alternation of surface area and pore size in clay-based materials for the adsorptive removal of contaminants from wastewater [20,21]. In pillared clays, exchangeable interlayer cations are replaced by polyhydroxy metal cations, which upon calcination form stable metal oxide pillars that expand interlayer spacing and generate porous structures with increased surface area and acidity.

A wide range of pillaring agents, such as aluminium, silicon, titanium, iron, boron, and zirconium polyhydroxy cations, have been employed to tailor the structural and surface properties of bentonite for environmental remediation and catalytic applications [22,23]. Among these, aluminium-pillared clays are well known for their high surface acidity and micro - mesoporous structure, while zirconium-pillared clays exhibit enhanced thermal stability and distinct surface chemical characteristics. Such materials have been applied for the removal of heavy metals, dyes, nutrients and even some pharmaceuticals. For instance, Chauhan et al. 2020 used Al-PILC to remove two antibiotics (amoxicillin and imipramine), achieving much higher adsorption capacities than with unmodified clay. Although pillared clays have demonstrated effectiveness in removing heavy metals, dyes, and selected pharmaceuticals, their application for β-lactam antibiotics, particularly ampicillin, remains insufficiently explored. In addition, systematic comparative studies evaluating aluminium- and zirconium-pillared bentonite under identical conditions are scarce. Furthermore, a critical gap exists in understanding how structural modification, particularly interlayer expansion and surface

functionalisation, likely governs adsorption performance and mechanism. Most existing studies focus primarily on adsorption capacity without establishing clear structure - performance relationships or considering practical feasibility.

Therefore, this study aims to understand how pillar chemistry (Al Vs Zr) controls the adsorption mechanism and performance of pillared bentonite prepared through a hybrid-assisted synthesis route, rather than simply demonstrating another adsorbent for ampicillin removal. The novelty of this work lies in elucidating how pillar chemistry (Al^{3+} versus Zr^{4+}) contributes to the evolution of interlayer architecture, surface acidity, pore development, and adsorption pathways in bentonite-based adsorbents prepared via a microwave-sonochemical hybrid synthesis route. Unlike previous studies that primarily report adsorption capacities, this work establishes quantitative structure - performance relationships that link physicochemical properties to adsorption behaviour toward β-lactam antibiotics. Furthermore, the applicability of the developed materials is evaluated using a representative hospital wastewater sample matrix and supported through regeneration and preliminary techno-economic assessment. Hence, the present study aims to establish a relationship with application in pillared bentonite systems by demonstrating how pillar chemistry (Al^{3+} vs Zr^{4+}) contributes to microstructural evolution, surface acidity, and adsorption pathways for β-lactam antibiotics.

2. Materials and Methodology

2.1.Materials

Bentonite Clay minerals were purchased from EMSTAR Materiały Budowlane, Szczecińska 9, 54-517 Wroclaw. Aluminium trichloride hexahydrate ($AlCl_3.6H_2O$ of 97% purity), Sodium hydroxide (NaOH), and Zirconium oxychloride ($ZrOCl_2$ of 96% purity) were purchased from Sigma Aldrich, USA. Ethanol (Merck, 99% purity) was obtained and used in the preparation of AlPC and ZrPC. Double-distilled water available in the laboratory, a

Cellulosic dialysis tube (Sigma-Aldrich, 33 mm), and Whatman filter paper were used wherever required during any process. An AMP drug of 500 mg was purchased from a chemist's shop made by J.R.S Oryx Pharmaceuticals Pvt. Ltd., India.

2.2.Synthesis of Adsorbents

2.2.1. AlPC: The adsorbent was synthesised following an adapted procedure based on Gil et al., incorporating a microwave-sonochemical hybrid method improving hydrolysis and intercalation possibilities. A solution of 1.5 M NaOH was slowly added to the 0.5 M $AlCl_3.6H_2O$ solution under continuous stirring, maintaining an OH/Al^{3+} molar ratio of 2.5 to promote the formation of aluminium polyoxocations. The obtained solution was subjected to controlled microwave-assisted ageing at 323.15 K for 36 h, with intermittent sonication applied to facilitate uniform hydrolysis and polymerisation of aluminium species. Afterwards, 5 g of finely ground bentonite (BT) was carefully introduced into the solution under ultrasonic dispersion to prevent accumulation and ensure homogeneous mixing. The suspension was further treated by combining mild microwave irradiation and sonication for 24 h to promote effective intercalation of aluminium polycations into the clay interlayers. The mixture was filtered using Whatman filter paper and centrifuged to recover the intercalated solid materials. The attained material was purified using a cellulose dialysis membrane to remove excess chloride and sodium ions, with dialysis continued until the electrical conductivity of the washing water decreased below 2 $\mu S\ cm^{-1}$. The purified sample was separated, dried at 373.15 K, and finally calcined at 773 K for 4 h to crop the AlPC adsorbent.

2.2.2. ZrPC: ZrPC adsorbent was synthesised following an optimised procedure, as testified in earlier studies with modifications, incorporating a microwave-sonochemical hybrid approach to enhance intercalation efficiency [24]. In this synthesis method, an aqueous solution of 0.1 M zirconyl chloride ($ZrOCl_2$) prepared in 50 mL of double - distilled water was added

dropwise to a well - dispersed suspension of bentonite clay (BT, 2.5 g), prepared earlier, in 250 mL under continuous stirring at room temperature. The addition was carried out under controlled ultrasonic irradiation to ensure uniform dispersion and to minimise local supersaturation, thereby suppressing premature precipitation of zirconium hydroxide species. The intercalation process was conducted at 313.15 K for 2.5 h, supported with mild microwave irradiation applied intermittently in combination with sonication to promote effective exchange of interlayer cations with zirconium polyhydroxy species while preserving the layered structure of the clay. Following intercalation, the suspension was filtered and centrifuged to recover the solid phase. The collected material was thoroughly purified as done with AlPC, wherein a cellulose dialysis membrane was used to remove the unreacted and excess ions or species. The washed and collected solid was dried in an oven at 373.15 K for 10 h. Subsequently, the dried sample was calcined at 623.15 K for 2.5 h to convert the intercalated zirconium species into stable zirconium oxide pillars, yielding the proposed ZrPC adsorbent.

2.3. Adsorbents Characterization

The specific surface area, pore volume, and pore size distribution of BT, AlPC, and ZrPC were determined via low-temperature N_2 adsorption–desorption measurements using a Micromeritics ASAP 2020 system. Before analysis, samples were degassed at 473 K for 2 h under vacuum. X-ray diffraction (XRD) patterns were recorded on a Bruker D8 Advance diffractometer equipped with Cu Kα radiation (λ = 1.5406 Å, 40 kV, 40 mA) over a 2θ range of 4°- 48° to assess basal spacing and crystallinity. Surface morphology was examined by scanning electron microscopy (SEM, Thermo Fisher Prisma E) with a resolution of 50 μm. Functional groups were identified using Fourier-transform infrared spectroscopy (FTIR, Shimadzu FTIR-8400) with the KBr pellet method, over a spectral range of 4000 - 400 cm^{-1}. The pHzpc was determined by equilibrating 0.05 g of each adsorbent in 100 mL of distilled

194 water at initial pH values ranging from 2 to 12, adjusted using 0.1 N HNO_3 or 0.1 N NaOH.
195 The suspensions were stirred continuously for 12 h at room temperature, after which the final
196 pH was measured and plotted against the initial pH to determine the pHzpc.

197 **2.4.Batch adsorption experiments**

198 Batch adsorption studies were carried out to evaluate and investigate the efficiency of BT,
199 AlPC, and ZrPC towards AMP. The influence of key operational parameters, including contact
200 time (up to 3 h), solution pH (2 - 12), temperature, and initial AMP concentration, was
201 systematically investigated. In addition, desorption and reusability studies were performed to
202 assess the regeneration potential of the adsorbents. All adsorption experiments were carried out
203 using a stock solution of AMP (1000 mg. L^{-1}), which was prepared by dissolving 500 mg of an
204 AMP capsule in double-distilled water. Wherein the amount of adsorbate adsorbed on the
205 adsorbent materials is calculated by using the following mass balance equation [25], expressed as
206 **Eq. 1** :

207 $$q_{ea} = \frac{C_i - C_e}{W} \times V \qquad \textbf{(1)}$$

208 Where C_i, mg. L^{-1} is the initial concentration, C_e, mg. L^{-1} is the final concentration, V stands
209 for volume in L, and W is the weight of the adsorbent in g, the q_{ea} is the adsorption capacity,
210 mg. g^{-1}.

211 The working solution of 200 mg. L^{-1} was prepared from a stock solution and made up to a
212 volume of 250 ml. The number of working solution sets was managed according to the batch
213 adsorption study. The interaction of adsorbent-adsorbate was performed at 200 rpm by adding
214 0.5 g of adsorbent. The solution was stirred in a water bath (fabricated using a transparent
215 container equipped with an inlet and outlet of water attached to a water bath) at 298 K with the
216 help of a magnetic stirrer with 15 multi-position to place the samples. The amount of adsorption
217 at various quantities was plotted to witness the time-based adsorption program. 5 ml of each

solution was filtered using a syringe filter (Fisher brand syringe filter Nylon 25 mm, 0.45 µm) and analysed using a UV-VIS spectrophotometer at 204 nm. The effect of pH on the adsorption of AMP molecules onto the BT, AlPC, and ZrPC was studied experimentally by making a solution of 11 different sets, each containing 200 mg. L^{-1} in 20 ml volume. The pH of the solution set ranged from 2 to 12. pH values were adjusted, and each value was fixed with 0.1 M HNO_3 and 0.1 N NaOH, wherever desired. After maintaining the pH, 0.04 g of adsorbent was added to each solution and placed on a stirrer cum water bath for 2 h of stirring.

2.5.Kinetics, modelling of adsorption data and thermodynamics

The adsorption efficiency of AMP onto BT, AlPC and ZrPC was assessed by the amount of AMP adsorbed from solution onto the adsorbent at equilibrium. This is evaluated by fitting the experimental data to the pseudo-first-order, pseudo-second-order and intra-particle diffusion model for the assessment of the adsorption mechanism. The pseudo-first-order equation is represented by **Eq. 2** [26].

$$\log(q_e - q_t) = \log q_e - \frac{k_1}{2.303} t \quad \textbf{(2)}$$

Where, k_1 (per hr) is the pseudo-first-order rate constant, q_e and q_t (mg. g^{-1}) are the amount of AMP adsorbed at equilibrium and time, respectively. The equation used in pseudo-second-order kinetics, **Eq. 3**

$$\frac{t}{q_t} = \frac{1}{k_2 q_e^2} + \frac{1}{q_e} t \quad \textbf{(3)}$$

Where, q_e and q_t (mg. g^{-1}) amount of adsorption at any time (t, h), k_2 (g. $mg^{-1}.h^{-1}$) is the pseudo-second-order adsorption rate constant, R^2 -correlation coefficients are determined by plotting t/q_t against t. The equation used for intra-particle diffusion is given in **Eq. 4**:

$$q = k_{id} t^{0.5} + C \quad \textbf{(4)}$$

Where k_{id} (mg^{-1}. min$^{-1/2}$) is the intra-particle diffusion rate constant, and C (mg. g^{-1}) is a constant in the intra-particle diffusion model, suggest the consequences of the boundary layer on mass transfer effect.

Meanwhile, to investigate and extract the information on the adsorption behaviours of AMP onto the adsorbents and the effect of temperature, two different adsorption models, namely Langmuir [27], and Freundlich [28], were examined.

In both models, the experimental data used are presented as a plot of q_e vs C_e, and the values of both parameters are calculated using the equations described below to assess the best fit. The Freundlich isotherm is represented by the following **Eq. 5**:

$$Log\ q_e = log\ K_f + \left(\frac{1}{n}\right) logC_e \quad \textbf{(5)}$$

Where: C_e (mg. L^{-1}) is the equilibrium concentration, q_e (mg. g^{-1}) is the amount adsorbed at a specific amount of adsorbent at equilibrium, K_f (mg. g^{-1}) is the constant which is the adsorption capacity, and n (mg. g^{-1}) is a constant which is the adsorption capacity.

Whereas the Langmuir isotherm equation is represented in the following form of **Eq. 6**:

$$\frac{C_e}{q_e} = \frac{1}{q_{max}b} + \frac{C_e}{q_{max}} \quad \textbf{(6)}$$

Where, q_e (mg. g^{-1}) is the amount of AMP adsorbed at equilibrium, C_e (m·g· L^{-1}) is the equilibrium concentration, q_{max} is the Langmuir constant related to the adsorption capacity, and b (L· mg^{-1}) is also a Langmuir constant which is related to the energy of adsorption.

In the present work, the adsorption thermodynamics of the AMP was investigated with the help of its adsorption isotherms on the three different temperatures (298, 308, and 318 K). The adsorption temperature is an important parameter as it controls the progress of an adsorption process. The thermodynamics of adsorption depends on the adsorbate-adsorbent interaction

and therefore varies from system to system. The practical applications of an adsorption process largely depend on the values of thermodynamic parameters. In this study, thermodynamic factors such as a change in Gibbs' free energy ($\Delta G°$), enthalpy ($\Delta H°$), and degree of entropy ($\Delta S°$) were calculated using the following **Eq. 7 - 9** [29]:

$$\Delta G° = \Delta H° - T\Delta S° \quad \textbf{(7)}$$

$$\Delta G° = -RT \ln Ka \quad \textbf{(8)}$$

$$InKa = \frac{\Delta S°}{R} - \frac{\Delta H°}{RT} \quad \textbf{(9)}$$

In these thermodynamically meaningful parameters, the Langmuir equilibrium constant (b, L. mg^{-1}) was converted into a dimensionless equilibrium constant (Ka) according to Ka = b*1000*MW, in which MW defines molecular weight.

Where R is a gas constant (8.314 $J \cdot mol^{-1} \cdot K^{-1}$), T (K) is the value of temperature, and K_a is the thermodynamic equilibrium constant. K_a is dimensionless, calculated by converting the Langmuir equilibrium constant (b) in units of L. mol^{-1}. As the isotherm data were reasonably explained with the Langmuir model, it is also reasonable to use the Langmuir equilibrium constant for the determination of ΔG°. The values of ΔG°, ΔH°, and ΔS° were calculated from the Van't Hoff plot of $\ln K_a$ versus 1/T.

2.6.Desorption & Reusability

Desorption and reusability are considered crucial aspects of the present work, where the reusability of exhausted adsorbent is inspected to reuse it several times. In the first instance, an appropriate desorbing agent is selected amongst the prescribed ones, which are Sodium Hydroxide (NaOH), Sodium Chloride (NaCl), Phosphoric Acid (H_3PO_4), Nitric Acid (HNO_3), Distilled water, and Hydrochloric Acid (HCl), to achieve maximum desorption. Secondly, the best performing desorbing agents are further used to desorb/ regenerate (removing AMP from

the pores of adsorbents) the exhausted material. Lastly, the adsorption and desorption of exhausted material is considered as cycle 1, and this process is repeated in a cyclic way until less than 50% adsorption capacity is retained. The desorption capacity is calculated using the formula given in **Eq. 10** [30].

$$q_{ed} = C_{ed} \times \frac{V}{w} \quad \textbf{(10)}$$

Where C_{ed} is the absorbance of the desorption solution, V is the volume in L, and W is the weight of the exhausted adsorbent in g.

Percentage desorption was calculated by using the formula given in **Eq. 11** [30].

$$\%\, Desorption = \frac{q_{ed}}{q_{ea}} \times 100 \quad \textbf{(11)}$$

Where q_{ed} is the desorption capacity, and q_{ea} is the adsorption capacity (mg. g^{-1})

3. Result and discussion

3.1. Structural and physicochemical characterisation

The structural modification of BT through Al^{3+} and Zr^{4+} pillaring resulted in significant changes in textural and surface properties, which are critical for adsorption performance. The relationship between structural evolution and adsorption behaviour is discussed below.

3.1.1. N_2 adsorption-desorption

The surface area and porosity specification of the adsorbent materials along with BT of Poland origin are calculated using N_2 adsorption-desorption analysis. The obtained isotherm of BT8 can be classified as Type II according to the IUPAC nomenclature of adsorption isotherms. This is the indication of a non-porous/ microporous structure with a flat surface. A distinct hysteresis loop of type H3 can be observed from Figure 1 in the relative pressure (P/P_0) in the range of 0.4 - 1.0. This suggests the availability of silt-shaped pores typically

associated with layered clay minerals such as bentonite. The BET specific surface area calculated using BET theory and determined to be 53 m^2. g^{-1}, whereas the total pore volume is calculated to be 0.11 $cm^3.g^{-1}$ with 0.001 $cm^3.g^{-1}$ volume of microporosity. These textural properties are attributed to the aluminosilicate structure of bentonite clay. The intercalation of many salts has changed the surface properties, resulting in increased surface area, pore volume, and microporosity. Here, chemically modified forms of AlPC and ZrPC exhibited significantly higher surface area, pore volume, and microporosity than raw BT. The resultant adsorption-desorption isotherm for AlPC is classified as Type IV according to the IUPAC nomenclature classification of adsorption isotherms. This indicates the availability of a well-organised mesoporous structure. The obtained results showed a H3/H4 hysteresis loop in the range of approximately 0.4-1.0 relative pressure (P/P_0). This suggest the existence of slit-shaped pores after aggregation of platelets of layered clay. The appearance of a type H4 indicates the presence of microporosity, attributed to the formation of stable interlayer galleries after aluminium pillaring. The appearance is shown in Figure 1a.

From the BET theory, the calculated specific surface area is 272 m^2. g, showing 5 times of surface area enhancement as compared to raw bentonite. This enhancement is a result of Al-polycations acting as pillars, which avoids layer collapse. The pore size distribution analysis, using the BJH method, measured an average pore diameter of 1.97 nm, indicating the existence of mesopores along with contributions from micropores [31], the details are summarised in **Table 1**. It is noteworthy here that most of this increase is contributed by the surge in microporous volume ($V\boldsymbol{\mu}$), which increased to 0.11 cm^3. g^{-1} in AlPC [32]. In addition, the total pore volume of AlPC increased to 0.17 cm^3. g^{-1}, demonstrating the formation of a hierarchical pore network.

Table 1: Surface area, pore volume, and 2θ of the BT and developed AlPC and ZrPC from different metal polyoxides

S.No	Sample	A_{BET} (^{2}. g^{-1})	V_{total} (cm^3. g^{-1})	V (cm^3.g^{-1})	D_{001} (nm)	2 θ, theta	Extended interlayered space (nm)
1	BT	53	0.11	0.001	1.05	8.39	0
2	AlPC	272	0.17	0.11	1.97	4.95	0.86
3	ZrPC	231	0.15	0.09	1.89	4.82	0.82

ZrPC also has textural enhancement relative to raw BT. The BET surface area increased to 231 m^2. g^{-1}, and revealing an approximately 80% increase in micropore volume (0.09 cm^3 g^{-1}), determined by the t-plot method. The total pore volume of the adsorbent material is 0.15 cm^3 g^{-1}, suggesting that zirconium pillaring promotes the formation of micropores and partially mesopores. The nitrogen adsorption-desorption isotherm possesses a hybrid type I(b)-type II(b) profile with an H3 hysteresis loop, as per the IUPAC classification [33,34]. The type I(b) isotherm confirms the wider microspores in this sample. whereas type II(b) mimics the interstitial pores and external structure of the prepared adsorbents, which are preserved and are not interrupted during intercalation. The narrow hysteresis loop results after inter-particle capillary condensation within non-rigid aggregates of clay particles [35].

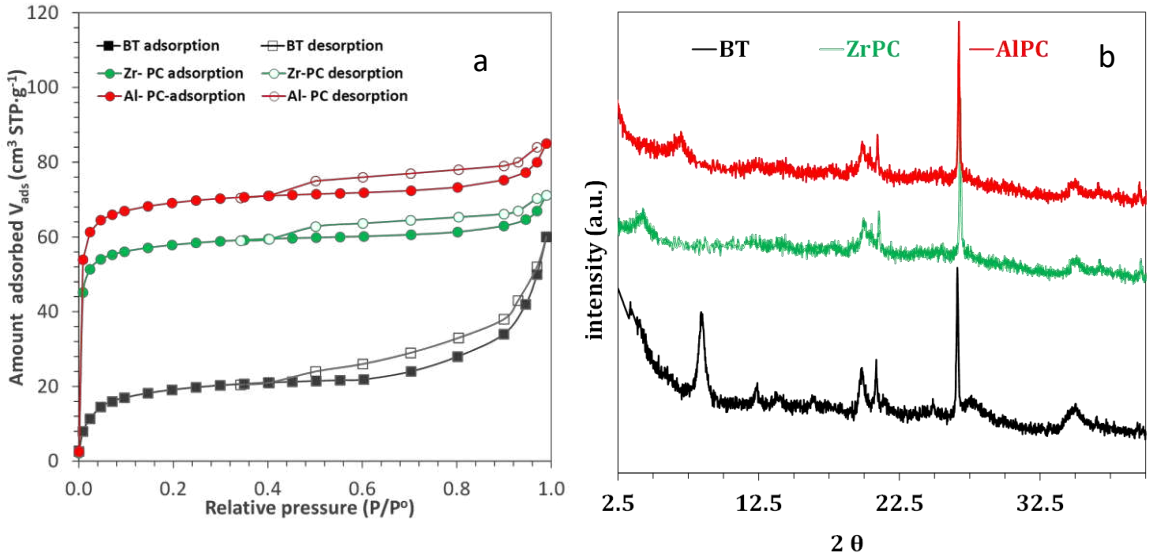


Figure 1: 1a. Nitrogen adsorption-desorption isotherms of BT and synthesised ZrPC, as well as AlPC. 1b. Shows the XRD pattern of BT, ZrPC, and AlPC

3.1.2. X-Ray Diffraction

The powder XRD patterns of the synthesised adsorbents and BT materials are recorded between 2.5 to 40° 2θ. **Figure 1b** illustrates that the 2θ value for the synthesised adsorbents shifted and decreased, as presented in **Table 1** (Manohar et al. 2006). The pillaring materials enhance the interlayer space and are fixed after calcination, as it's expected to have an extension in *d*-spacing. The measured d_{001} value for the BT is 1.05 nm at 8.37 °2θ, whereas the peak is decreased for calcined AlPC and ZrPC; hence, no evidence of this peak is observed. This also supports the successful intercalation of the polycations. Additionally, the basal reflections shift to lower diffraction angles, with 2θ values of 4.95° for AlPC and 4.82° for ZrPC. The corresponding d_{001} spacings for the materials are calculated using Bragg's equation ($2d \sin\theta = \lambda$, $\lambda = 0.15$ nm), increasing to 1.87 nm for AlPC and 1.79 nm for ZrPC, confirming the considerable expansion in the interlayer. The amount of expansion can be calculated by subtracting 0.93 nm (thickness of the clay layer). The extended interlayered spacing of AlPC was calculated as 0.86 nm, and ZrPC as 0.82 nm [37] [38]. This expansion facilitates the diffusion

and accommodation of AMP molecules within the clay galleries, thereby improving adsorption capacity. The conservation of the clay structure after amendment further indicates that pillaring improves functionality without structural degradation.

3.1.3. ***Scanning Electron Microscope (SEM)***

The morphological evolution of bentonite following pillaring was investigated using scanning electron microscopy (SEM), and the corresponding micrographs are presented in **Figure 2**. Pristine bentonite (BT) exhibits a compact morphology characterised by stacked plate-like particles with relatively smooth surfaces and dense aggregation, which is typical of layered montmorillonite clay minerals. The closely packed lamellar arrangement suggests limited accessibility to internal adsorption sites and restricted pore development. Following pillaring with Al and Zr polycations, substantial modifications in surface morphology were observed. Both AlPC and ZrPC display a markedly more open and disordered architecture consisting of loosely packed flakes, expanded lamellae, and interconnected porous networks. The pillared samples exhibit increased surface roughness and reduced particle aggregation, indicating successful intercalation of metal polycations within the interlayer galleries. During the pillaring process, the introduction of positively charged Al and Zr species promotes interlayer expansion and partial delamination of the clay sheets through electrostatic interactions, resulting in a more accessible porous framework. Related to pristine BT, the pillared materials exhibit a less compact and more thermally stabilised structure, reflecting the formation of stable oxide pillars that prevent layer collapse during calcination. The observed morphological transformation is consistent with the XRD results, which revealed a significant increase in basal spacing, and with BET analysis, which revealed enhanced surface area and pore volume following pillaring. The development of a rough, porous, and expanded lamellar structure is expected to facilitate mass transfer, increase the availability of active adsorption

sites, and improve the diffusion of ampicillin molecules into the interlayer and pore regions. The SEM observations are further supported by EDX analysis (Figure 2 (d - f)), which confirms the presence of the principal framework elements, including O, Si, Al, Mg, K, and Fe. Notably, the increased Al content in AlPC and the appearance of Zr signals in ZrPC provide direct evidence for the successful incorporation of pillar-forming species into the bentonite structure. The compositional changes observed by EDX, together with the morphological evolution identified by SEM, corroborate the successful formation of pillared clay architectures responsible for the enhanced adsorption performance of the modified materials. Similar results were obtained [39] with AlPC [40] and ZrPC, respectively.

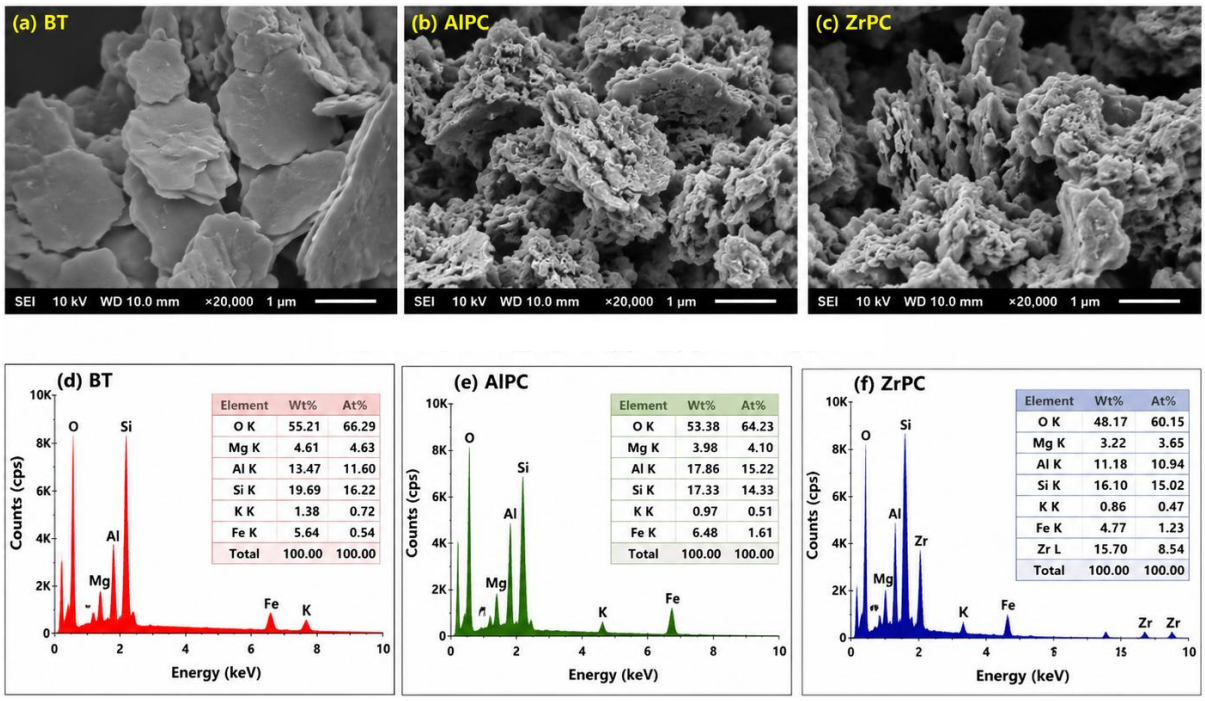


Figure 2: SEM micrographs a - c, EDX spectra d - f, and elemental composition of pristine bentonite (BT), AlPC, and ZrPC. The pillared samples exhibit a rougher and more porous morphology compared with BT, while EDX analysis confirms the incorporation of Al and Zr species and the preservation of the clay framework elements after pillaring.

3.1.4. ***Fourier-Transform Infrared Spectroscopy (FTIR)***

FTIR spectra for BT, AlPC, and ZrPC are presented in **Figure 3**. In the high-frequency region (3350 - 4000 cm^{-1}), the wide absorption peak in BT represents the stretching of interlayer water and structural -OH coordinated with octahedral Al. The decline in intensity or disappearance of this peak in the developed adsorbents signifies dehydration or replacement of the interlayer water with inorganic polycations. The symmetric O-H stretching vibrations for H-bonded water have been seen in the 3450 cm^{-1} peak. There is an extra peak for adsorbents at 3652 cm^{-1} because of the shifting of the SiOH group within the BT structure. Due to pillaring with oxide pillars, these Si-OH groups were shifted and labelled as SiOH. The bands appearing at 550 $cm^{-}1$ and 1000 cm^{-1} are due to Al-O and Zr-O stretching vibrations, which signify the formation of pillars due to the pillaring effect. The peak appearing at 1556 cm^{-1} in AlPC has increased intensity compared to BT because of increased water content due to the intercalation of Al-polycations. The peak appeared within the range of 540-450 cm^{-1} due to Si-O bending and Al-O stretching vibrations. There was no shift in Si-O bending vibrations, while a slight increment in intensity has been noticed in Al-O stretching vibrations, which can be due to Al salts of OH^{-} /Al^{3+}. This point has also been supported by the findings of [41]. Some new bonds can be observed between 400 and 430 cm^{-1} in ZrPC, which may be attributed to the presence of Zr-O bonds and the same argument is also supported by [42,43].

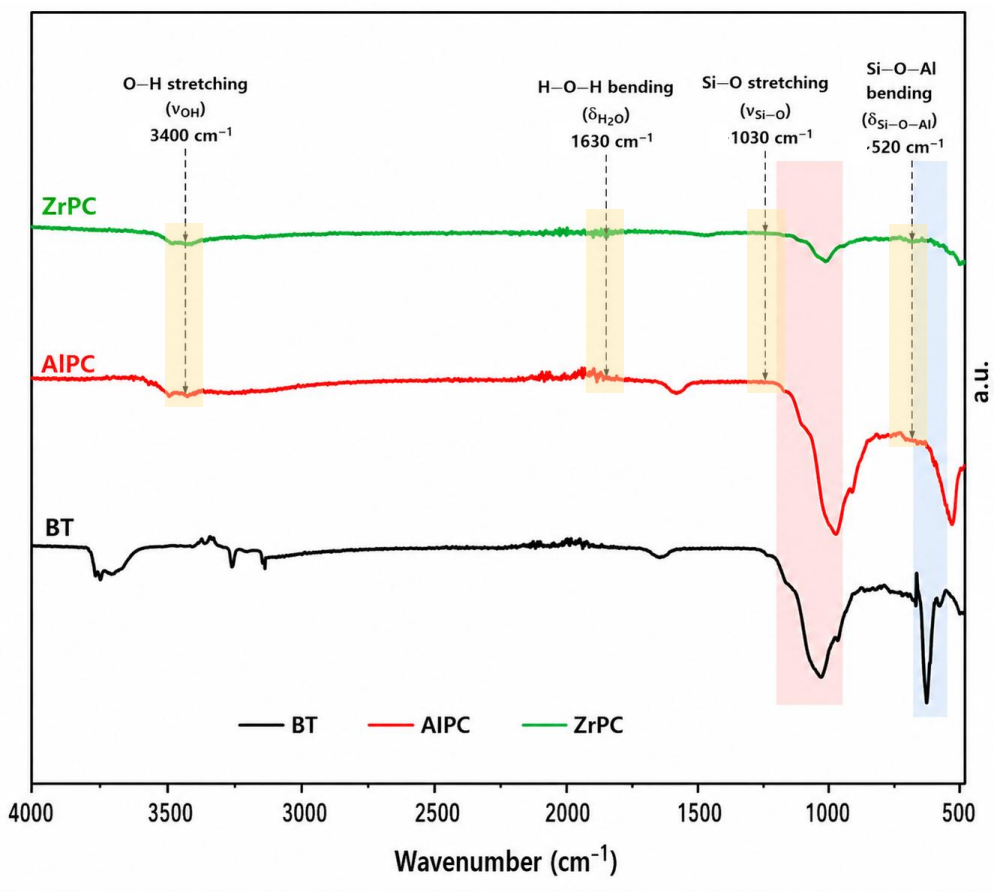


Figure 3: FTIR pattern of BT and synthesised clay adsorbent as AlPC and ZrPC

3.1.5. pH_{zpc}

The pH_{zpc} is well-defined as the pH of the solution wherein the surface charge density of the material is zero. The presence of charge over the surface of the adsorbents and adsorbate changes according to the pH of the solution, shown in **Figure 4**. This plays a vital role in the removal of contaminants from wastewater. Further, the pH of the solution determines the presence of a partially positive or negative charge over the surface, which consequently controls the interaction between the adsorbent and adsorbate. Therefore, it is imperative to measure the effective charge over the adsorbent surface using a point of zero charge (pH_{ZPC}). This exposes the pH value where the net charge on the adsorbent surface in the solution is equal to zero. Wherein, the value of pH < pH_{ZPC} determines the surface of the material remains

positively charged, whereas it gets negatively charged at the value of pH > pH_{ZPC}. These are the chemical characteristics of the adsorbents which regulate the attractive or repulsive interactions between the adsorbent surface and the adsorbate, and the analysed pH_{ZPC} is shown in Figure 4 with a plot of initial pH values versus final pH values. The pH_{ZPC} value for the BT was determined as 7.9, which changed after the intercalation, resulting in 6 for AlPC and 5.8 for ZrPC. The oxide pillars in the interlamellar region helped increase the clay's acidic properties. Further, it may be concluded that the surface of the materials will be positively charged under neutral pH, and above this pH, it will be negatively charged. In acidic conditions, the BT and adsorbents show low adsorption, which may be due to the interaction of the protonated form of AMP with the protonated surface (partially positively charged) of the material being less. Further deprotonation of the AMP increases as pH increases, which offers more interaction with the surface because of electron-rich groups like -COO-, $-NH_2$, and -OH. It can be observed that the interaction is favoured by weak dipole interaction, hydrogen bonding, π- π interaction, and electrostatic interactions.

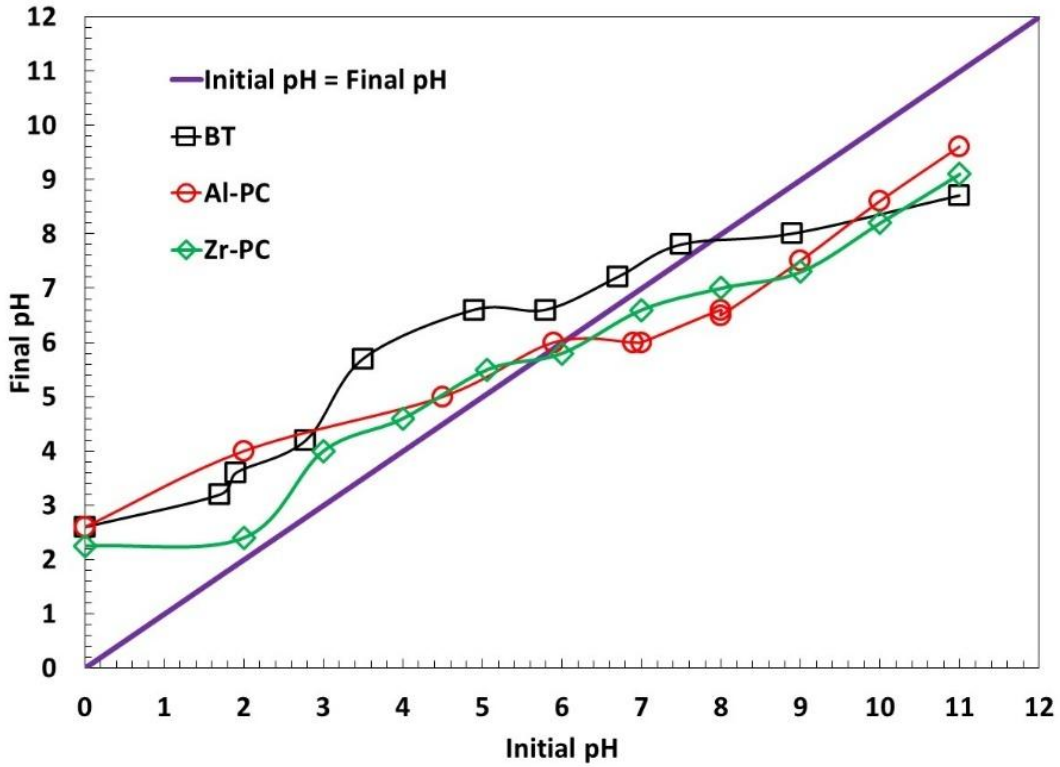


Figure 4: pH_{ZPC} graph for the BT, AlPC and ZrPC

3.2.Batch Adsorption Studies

3.2.1. Effect of contact time and kinetic study

In the adsorption process, adsorbents accomplish their maximum or become saturated after a specific time, known as equilibration time. This observation determines the equilibrium point where the adsorption and desorption rates are equal in an adsorbate-adsorbent interface system. The interaction of the AMP compound with the liquid-solid interface from the liquid phase was projected by changing the contact time from 1 to 180 min. The results are presented in **Figure 5a**, demonstrating the rapid initial adsorption and upsurges with time until the adsorbents: BT, AlPC, and ZrPC achieve the optimal removal efficiency. In the present study, adsorbents reached maximum adsorption within about 20 min at 298 K, then the adsorption process slowed. showed a slow process. Eventually reaching a plateau where none of the adsorbent material can be removed under the given conditions. The methodology was already discussed

in section 2.4, and the adsorption capacity is calculated with **equation 1**. The maximum adsorption capacities at 298 K follow the order 73.67 mg·g^{-1} for AlPC, 59.17 mg·g^{-1} for ZrPC, and 16.17 mg·g^{-1} for pristine BT. The fast initial adsorption is attributed to the availability of abundant active sites and high surface reactivity, and surface area, particularly in pillared clays. Further, the adsorption rate gradually decreases with time, where the adsorption-desorption phenomena prevail simultaneously. The experimental data were described by the pseudo-second-order kinetic model (for AlPC = 0.997, ZrPC = 0.98, and BT = 0.99), explained in **Figure 5b**, indicating that the adsorption process is likely governed by the availability of active adsorption sites and surface interactions. However, the good agreement with the pseudo-second-order model does not necessarily imply a purely chemisorption-controlled mechanism. Instead, the adsorption process is likely influenced by the combined effects of diffusion and surface interactions.

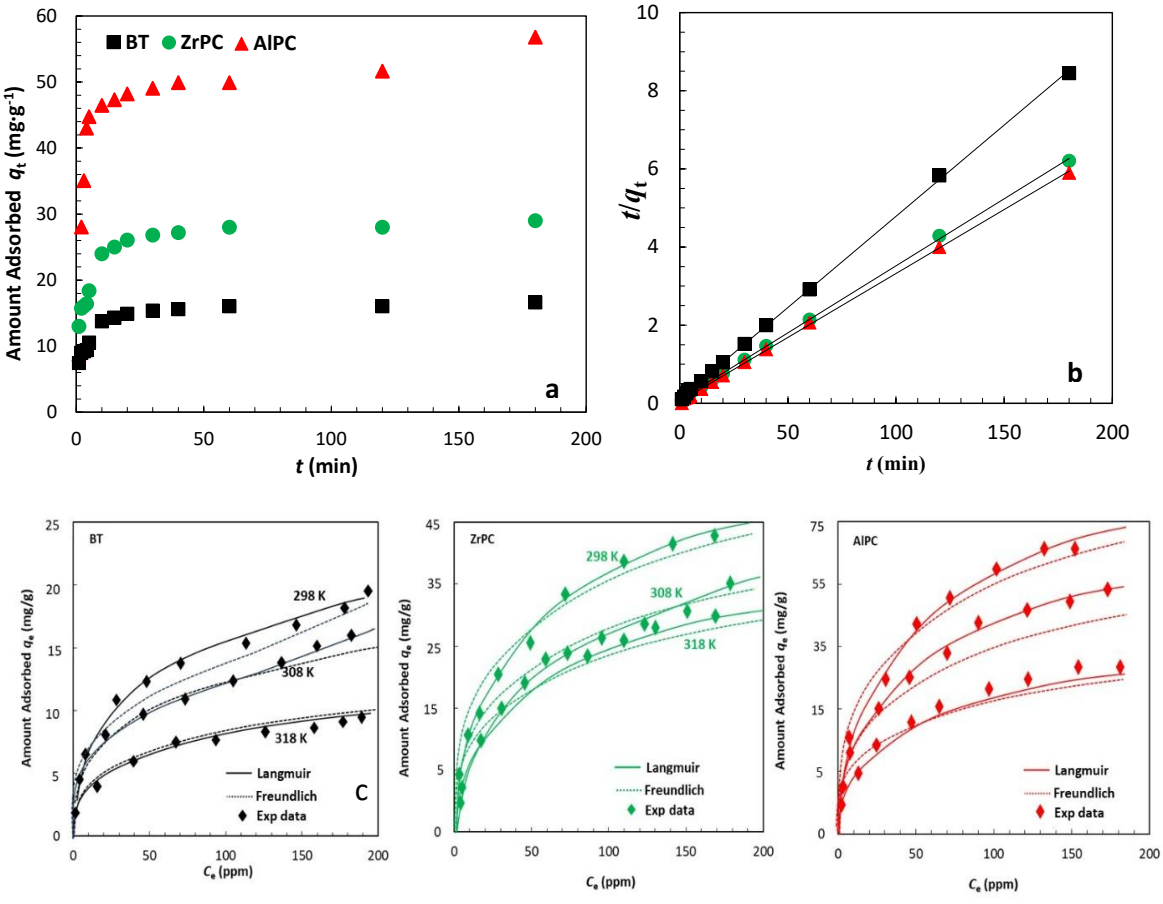


Figure 5: Effect of contact time (5a) and kinetics (5b) on the adsorption capacity of BT and the synthesised adsorbent materials at 298K. Whereas the effect of different temperatures and isotherm modelling on the adsorption capacity of BT, ZrPC, and AlPC (5c).

3.2.2. Effect of pH

The pH of the solution leads to the adsorption of the AMP molecule onto the adsorbent surface by determining whether the molecules are protonated or deprotonated. Likewise, the surface charge of the adsorbents is also altered with the pH of the solution, according to the pH_{zpc} of the adsorbent. The adsorption of AMP on BT, AlPC, and ZrPC is presented in **Figure 6**, which shows variation in the amount of adsorption of AMP, as a function of its solution pH. The adsorption of AMP molecules on AlPC and ZrPC is high at pH 2.0 as compared with the BT because at this pH, AMP remains in its molecular form and has electron-rich groups like amine and hydroxyl, which inspire its interaction with adsorbents at this pH [44,45]. Further, an increase in pH decreases the positive charge in AlPC and ZrPC, which causes a minor reduction in adsorption up to pH 7. Next, beyond pH 8 causes an increase in adsorption capacity, possibly due to the dimerisation of AMP molecules, as reported by other researchers [46]**.** Hence, the maximum adsorption of AMP on AlPC and ZrPC is observed between pH 10 and pH 11 (alkaline conditions), where increased deprotonation of AMP boosts interaction with the adsorbent surface. These results suggest that electrostatic interactions and hydrogen bonding are foremost in adsorption, particularly in pillared systems with improved surface functionality.

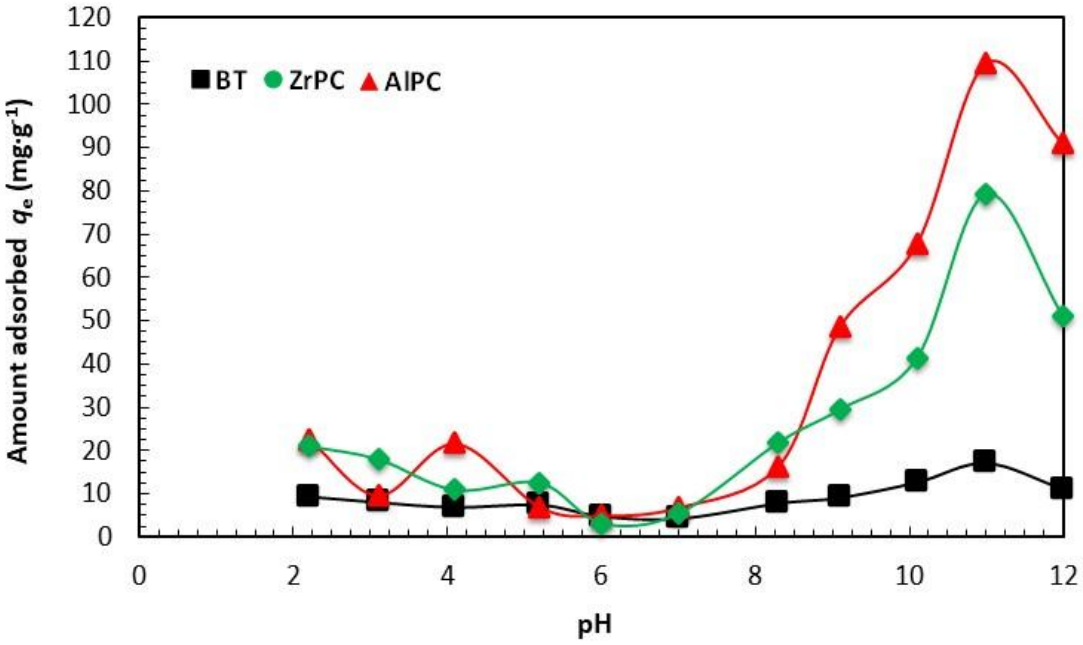
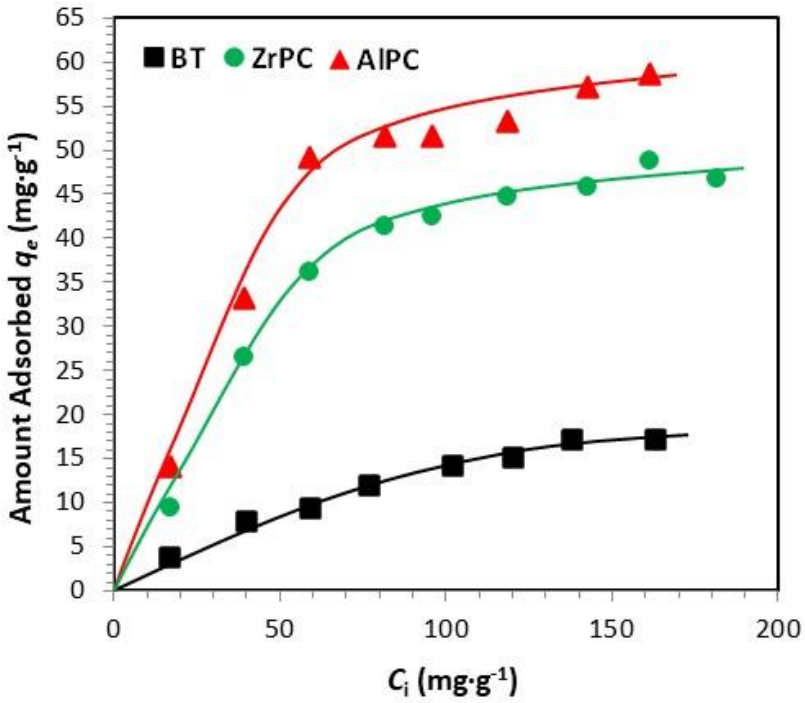


Figure 6: Effect of pH on the adsorption capacity of the starting material and pillared clays at 298K

3.2.3. Effect of Initial Concentration

To evaluate and assess the effect of initial concentration on adsorption, the initial concentration of AMP was varied between 20 - 200 mg. $L^{-1,}$ whereas the rest of the parameters remained unchanged. The graph plotted between the initial concentration, $q_{i,}$ *vs* the amount of AMP adsorbed, c_e (**Figure 7**)**,** shows that the concentration is directly proportional to adsorption up to a certain limit or until the equilibrium is achieved. The possibility of this phenomenon is due to the augmentation in the mass gradient pressure between the adsorbate and the adsorbent, which is the cause of the movement of the AMP molecule from the bulk solution to the surface of the adsorbents. Moreover, the initial concentration of the AMP increases the number of collisions between the analyte molecule and the adsorbents [47,48].



505

506 **Figure 7: Effect of initial concentration on different adsorbent materials developed from**
507 **clay**

508 ***3.2.4. Adsorption isotherm and thermodynamics***

509 The equilibrium adsorption behaviour of AMP onto BT, AlPC, and ZrPC was investigated
510 at different temperatures (298, 308, and 318 K), and the corresponding isotherm parameters
511 are summarised in **Table 2**. Among the tested models, the Langmuir isotherm provided the
512 best fit to the experimental data, as evidenced by the higher correlation coefficients compared
513 with the Freundlich model. This finding suggests that adsorption predominantly occurs
514 through the formation of a monolayer on relatively homogeneous adsorption sites (Roca Jalil
515 et al. 2017).

516 The maximum adsorption capacities obtained from the Langmuir model decreased with
517 increasing temperature for all adsorbents, indicating that adsorption is thermodynamically
518 favored at lower temperatures. At 298 K, AlPC exhibited the highest adsorption capacity

519 (73.67 mg g^{-1}), followed by ZrPC (59.17 mg g^{-1}) and pristine bentonite (16.17 mg g^{-1}). The
520 superior adsorption performance of AlPC can be attributed to its larger specific surface area,
521 higher micropore volume, and greater interlayer expansion, which provide improved
522 accessibility to active adsorption sites. The favorable fitting of the Langmuir model implies
523 that adsorption mainly occurs on energetically similar sites distributed throughout the
524 adsorbent surface. The enhanced adsorption capacities observed for pillared clays relative to
525 pristine bentonite further validate the beneficial role of pillar-induced structural modification
526 in promoting the uptake of ampicillin molecules. The results are presented in **Figure 5c**) to
527 interpret the interaction of adsorbed species with the adsorbent surface at a particular
528 temperature.After fitting the models, the parameters obtained from non-linear fittings of the
529 above equations on isotherm data are compiled in **Table 2**.
530

531 **Table 2: Langmuir and Freundlich parameters of the adsorption modelling obtained with**
532 **raw clay material and developed pillared clay materials, at different temperatures**

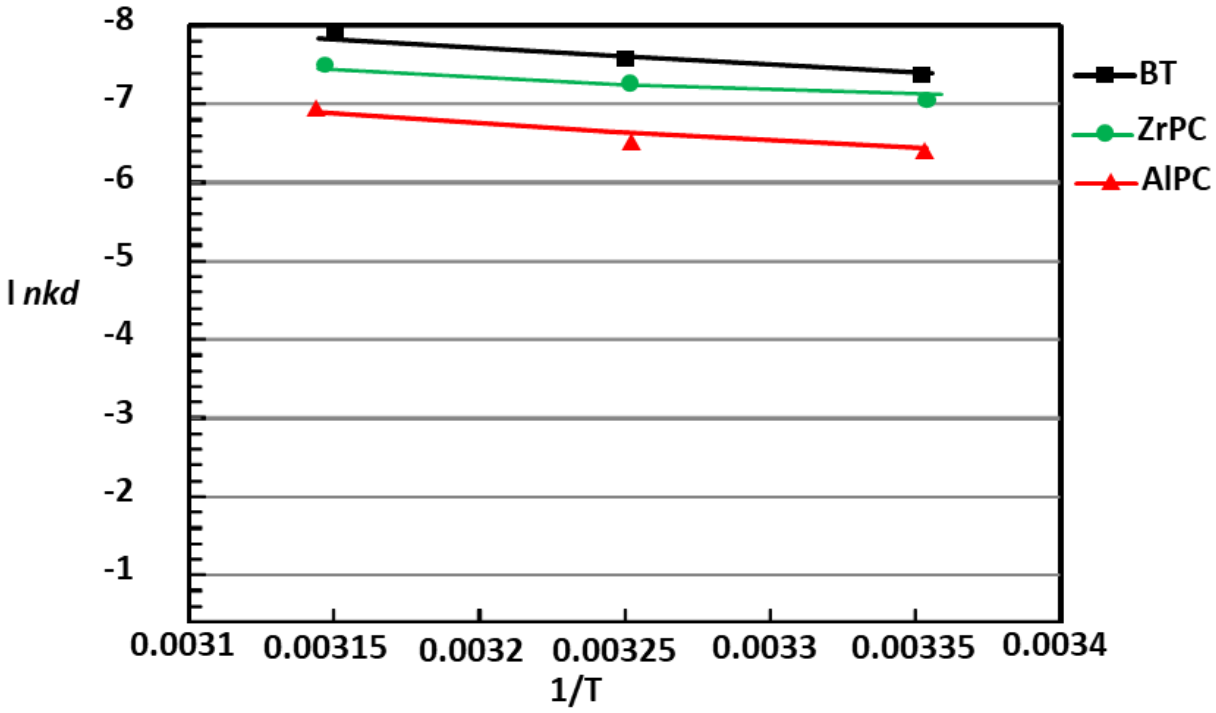
Sample	Temp (K)	Langmuir fitting parameters			Freundlich fitting parameters		
		q_{max}	B	R^2	K_f	1/n	R^2
		($m.g^{-1}$)	($L.mg^{-1}$)	-	($m.g^{-1}$)	-	-
BT	298	16.17	0.04	0.9561	1.41	0.4	0.9227
	308	15.87	0.03	0.9660	0.95	0.46	0.9469
	318	7.28	0.02	0.9374	0.66	0.54	0.8388
AlPC	298	73.67	0.14	0.9961	11.31	0.28	0.8471
	308	42.14	0.12	0.9986	9.56	0.24	0.9014
	318	21.45	0.1	0.9532	6.16	0.27	0.7622

ZrPC	298	59.17	0.711	0.9884	8.12	0.276	0.8496
	308	36.55	0.41	0.9461	5.59	0.281	0.815
	318	18.39	0.019	0.8966	1.41	0.399	0.7644

Thermodynamic parameters, including the Gibbs free energy change (ΔG°), enthalpy change (ΔH°), and entropy change (ΔS°), were calculated to assess the spontaneity and energetic characteristics of the adsorption process. The thermodynamic parameters were determined using the equations described in the methodology section, and the calculated values are summarized in **Table 3**. Furthermore, the Van't Hoff plots of lnK versus 1/T are presented in **Figure 8**. The negative values of ΔG° obtained for all adsorbents indicate that adsorption proceeds spontaneously within the investigated temperature range. Moreover, the magnitude of ΔG° values suggests that adsorption is energetically favorable under ambient conditions. The negative values of enthalpy change (ΔH°) shows the exothermic nature of adsorption. This observation is in agreement with the experimental results, where adsorption capacity decreased as the temperature increased. The release of heat during adsorption suggests favourable interactions between AMP molecules and the active sites present within the pillared clay framework. Furthermore, the relatively low magnitude of ΔH° indicates that adsorption is predominantly contributed to by physical interactions rather than strong chemical bond formation. Such behaviour is consistent with the rapid adsorption equilibrium observed within 20 min, the successful regeneration of the adsorbents, and the adsorption mechanism proposed in this study. The entropy change (ΔS°) provides information regarding the degree of disorder at the solid - liquid interface during adsorption. The negative entropy values indicate a reduction in randomness as AMP molecules become adsorbed and confined within the expanded interlayer galleries and porous network of the pillared clays. This decrease in entropy

554 can be attributed to the ordered arrangement of adsorbed AMP molecules and the restriction of
555 their translational mobility upon adsorption. The structural confinement generated by the Al
556 and Zr oxide pillars contributes to the stabilisation of adsorbed molecules within the porous
557 framework.

558



559

560 **Figure 8: The Van't Hoff plots for the valuation of thermodynamic parameters for the**
561 **adsorption of AMP onto BT, AlPC, and ZrPC at different temperatures (298, 308 and**
562 **318K).**

563

564 The magnitude of ΔH° can provide valuable information regarding the adsorption mechanism.
565 Previous studies have reported that physical adsorption is generally associated with enthalpy
566 changes below approximately 30 - 40 kJ. mol^{-1}, whereas chemisorption typically exhibits
567 significantly larger enthalpy values (>80 kJ. mol^{-1}) Zhang et al. (2023c) and Mazen S. F. Al-
568 Hazeef (2024). In the present study, the relatively low enthalpy values obtained for AlPC and

ZrPC suggest that the adsorption process is predominantly contributed by physisorption. These findings are consistent with the pore-filling behaviour and electrostatic interactions inferred from adsorption isotherms and structural characterization. Nevertheless, considering the pseudo-second-order kinetic behaviour, the heterogeneity of the adsorbent surface, and the XPS evidence presented in this study (discussed in the later section), the contribution of specific surface interactions such as hydrogen bonding and Lewis acid-base coordination cannot be neglected. Therefore, the adsorption of ampicillin onto the pillared clays can be described as a synergistic process involving predominantly physical adsorption accompanied by minor chemisorption contributions. These observations further emphasise the importance of the engineered pillared architecture in enhancing the adsorption performance of the developed materials.

Table 3: Thermodynamic parameters for the AMP adsorption on AlPC and ZrPC

Sample	T (K)	ΔG° (kJ. mol^{-1})	ΔH° (kJ. mol^{-1})	ΔS° (J. mol^{-1}. K^{-1})
AlPC	298	-21.73	-13.24	-28.50
	308	-21.45		
	318	-21.16		
ZrPC	298	-22.08	-24.85	-9.30
	308	-21.99		
	318	-21.89		

3.2.5. Desorption and Reusability Study

After the batch adsorption studies, the evaluation of adsorbent regeneration and reusability is essential for assessing its practical applicability in industrial wastewater treatment. Regeneration of exhausted adsorbents through ozonation, thermal treatment, H_2O_2-based oxidation, microwave-assisted regeneration, wet peroxide oxidation, UV/H_2O_2 oxidation, or electrochemical processes often suffers from high energy consumption, operational complexity, and increased treatment costs [50]. The results revealed that 0.1 N NaOH was the most effective desorbing agent, achieving desorption efficiencies of approximately 97.5%, 95%, and 80% for BT, AlPC, and ZrPC, respectively, shown in **Figure 9a**. HNO_3 also exhibited considerable desorption performance, with desorption efficiencies of 81%, 79%, and 78% for BT, AlPC, and ZrPC, respectively. In contrast, H_2O showed the lowest desorption efficiency, indicating that the adsorption of AMP was not solely contributed by weak physical interactions. Based on these findings, NaOH preferred as desorbing agent and subsequently employed in the reusability experiments.

The regeneration performance of BT, ZrPC, and AlPC was evaluated over three consecutive adsorption - desorption cycles, and the results are presented in **Figure 9b**. A gradual decrease in adsorption and desorption efficiencies was observed for all adsorbents with increasing cycle number, indicating partial blockage of adsorption sites and incomplete desorption of strongly retained AMP molecules. For BT, the adsorption efficiency decreased from 100 ± 2.4% in the first cycle to 78 ± 2.2% and 55 ± 2.3% in the second and third cycles, respectively, while the corresponding desorption efficiencies decreased from 65 ± 2.3% to 52 ± 2.1% and 40 ± 1.9%. Similarly, ZrPC retained adsorption efficiencies of 100 ± 2.1%, 85 ± 2.1%, and 72 ± 2.0% over the three successive cycles, whereas the desorption efficiencies declined from 68 ± 2.2% to 60 ± 1.9% and 53 ± 2.0%. Among the investigated adsorbents, AlPC exhibited the highest regeneration stability, maintaining adsorption efficiencies of 100 ± 2.0%, 90 ± 1.8%, and 80 ±

1.9% after the first, second, and third cycles, respectively, with corresponding desorption efficiencies of 70 ± 2.1%, 63 ± 2.0%, and 57 ± 1.9%.

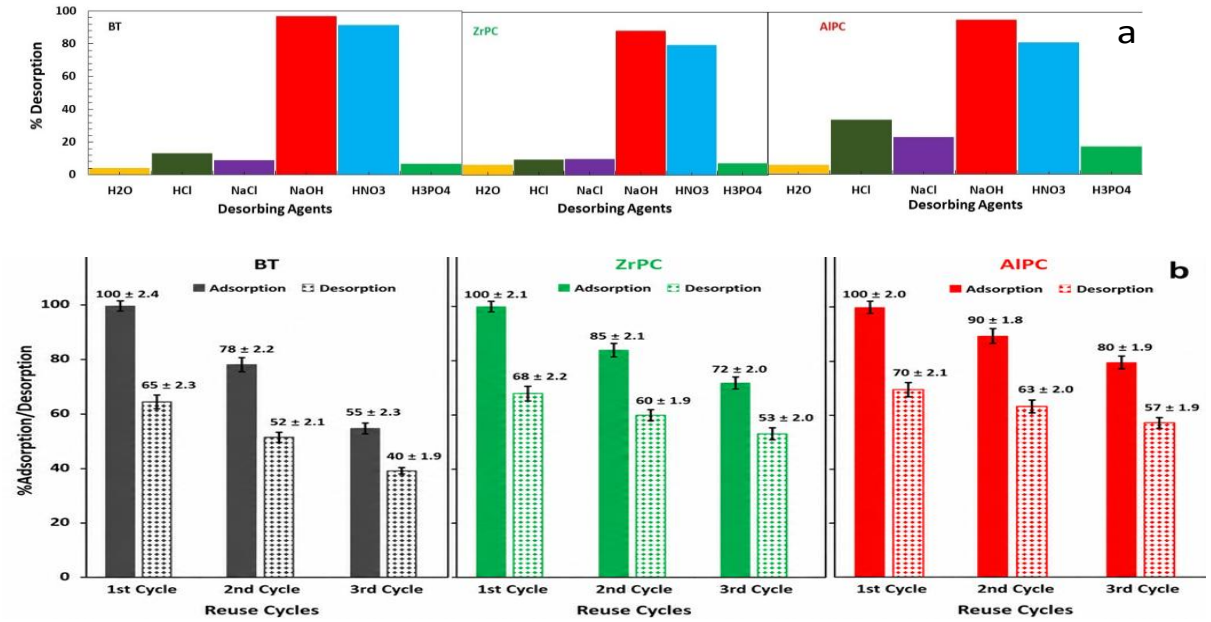


Figure 9: 9a. Effect of different desorbing agents on the extent of desorption from exhausted samples of BT, AlPC, and ZrPC. 9b. Test of reusability of prepared pillared clay materials with NaOH, up to 3 consecutive adsorption/desorption cycles.

The reusability of AlPC and ZrPC compared with BT can be attributed to the enhanced structural stability provided by the Al- and Zr-oxide pillars. These pillars preserve the expanded interlayer spacing and porous architecture during repeated adsorption - desorption operations, thereby maintaining a larger fraction of accessible adsorption sites. Although a gradual decline in adsorption performance was observed after repeated regeneration cycles, both pillared clays retained more than 70% of their initial adsorption efficiency after the third cycle, demonstrating their good operational stability and potential applicability for repeated wastewater treatment processes. It may be concluded that the reusability results suggest that pillaring improved regeneration performance under the tested conditions of bentonite, with AlPC exhibiting the highest long-term stability among the studied adsorbents.

3.3. Proposed adsorption mechanism of AMP on modified BT and molecular confinement

The adsorption of AMP onto AlPC and ZrPC is governed by the combined contributions of electrostatic interactions, hydrogen bonding, Lewis acid-base interactions, and pore-filling effects within the expanded micro-mesoporous framework generated after pillaring. The proposed adsorption pathways are illustrated in Figure 10, while XPS analyses (**Figure 11**) provide complementary evidence for the participation of surface functional groups and metal centers during adsorption. Pillaring with Al^{3+} and Zr^{4+} polyhydroxy species followed by calcination resulted in the formation of stable metal oxide pillars and enlarged interlayer galleries, leading to higher surface area, increased pore volume, and enhanced accessibility of adsorption sites. The expanded interlayer spacing of AlPC (1.87 nm) and ZrPC (1.79 nm) facilitates the diffusion and accommodation of AMP molecules within the clay galleries, thereby promoting adsorption.

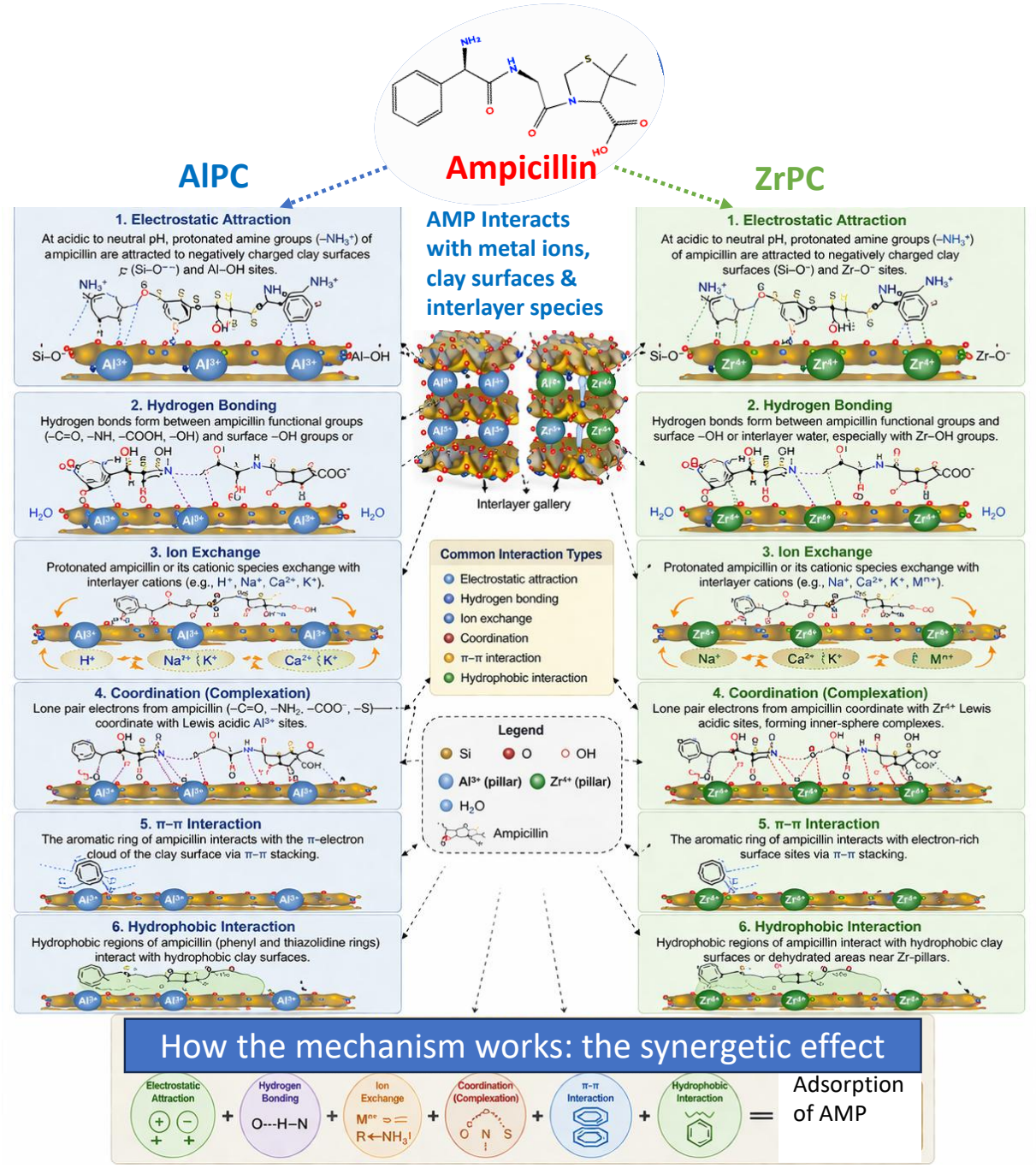


Figure 10: Adsorption mechanism of AMP molecules onto the clay surfaces, metal ions, and interlayer species of the AlPC and ZrPC adsorbent.

Electrostatic interactions constitute one of the principal driving forces for adsorption. The pHpzc values of AlPC (6.0) and ZrPC (5.8) indicate that the surface charge of the adsorbents is strongly pH-dependent. At pH values above pHpzc, deprotonated ampicillin species containing carboxylate groups interact with positively polarized hydroxylated Al and Zr sites.

Under acidic conditions, protonated amino groups of AMP may interact with negatively charged oxygen-containing surface species. Such electrostatic interactions facilitate the initial attachment of AMP molecules to the adsorbent surface.

Hydrogen bonding is likely an important contributor to adsorption owing to the abundance of surface hydroxyl groups associated with silanol species and hydroxylated metal oxide pillars. These hydroxyl groups may act as hydrogen-bond donors or acceptors and interact with amino ($-NH_2$), hydroxyl (-OH), carboxylate ($-COO^-$), and β-lactam carbonyl groups present in ampicillin molecules. The coexistence of multiple functional groups in AMP allows the formation of several hydrogen-bonding configurations, thereby enhancing adsorption stability.

In addition to electrostatic attraction and hydrogen bonding, Lewis acid-base interactions may contribute to the adsorption process. Hydroxylated Al^{3+} and Zr^{4+} species act as Lewis acid sites capable of interacting with electron-rich functional groups present in AMP molecules. Electron donation from oxygen-containing groups of AMP to partially vacant orbitals of Al and Zr centres may contribute to the stabilisation of adsorbed species. However, these interactions are inferred from spectroscopic observations and should be regarded as possible coordination interactions rather than definitive evidence of inner-sphere complex formation.

The XPS analyses shown in Figure 11 support the occurrence of surface interactions after adsorption. The appearance of the N 1s signal following adsorption indicates the immobilisation of AMP molecules on both adsorbents. Furthermore, slight shifts observed in the O 1s spectra indicate changes in the chemical environment of hydroxyl and lattice oxygen species after adsorption. Similar changes were observed in the Al 2p and Zr 3d spectra, suggesting modifications in the electron density surrounding the metal centers. These spectral variations imply the involvement of hydroxyl groups and metal oxide pillars in the adsorption process.

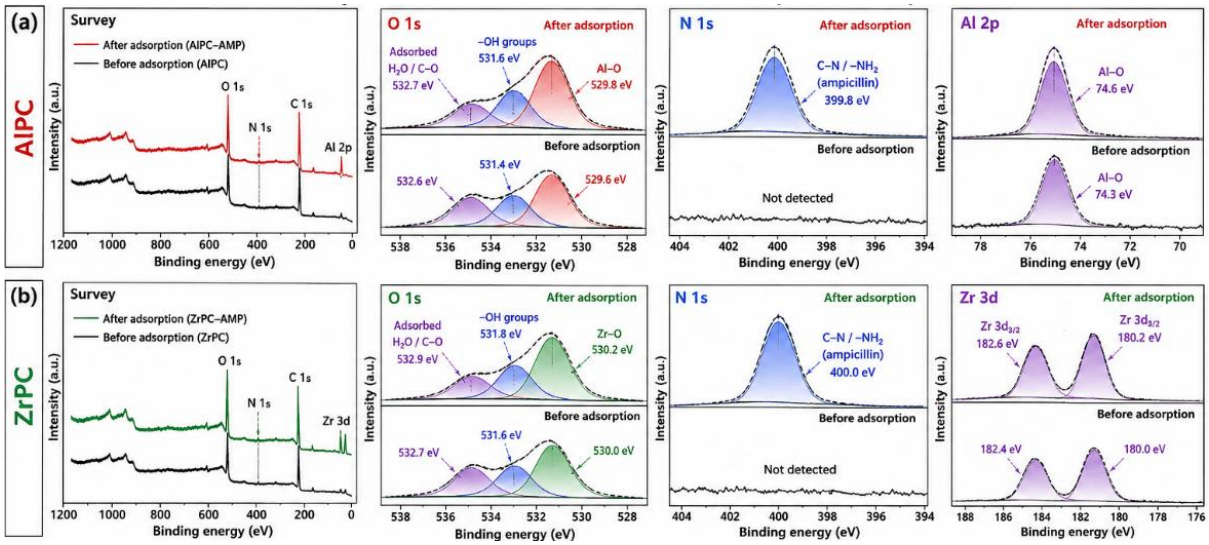


Figure 11: XPS survey and high-resolution spectra of (a) AlPC and (b) ZrPC before and after adsorption of AMP molecules.

To further clarify the proposed adsorption mechanism, FTIR spectra were recorded before and after adsorption, and the corresponding spectra are presented in Figure 12. Both adsorbents exhibited characteristic vibrations of the pillared clay framework before adsorption, including the broad O-H stretching band at approximately 3430-3440 cm^{-1}, assigned to structural hydroxyl groups and adsorbed water molecules, the weak aliphatic C-H stretching vibration near 2920 cm^{-1}, the H-O-H bending vibration around 1630 cm^{-1}, the intense Si-O stretching vibration centred at approximately 1030 cm^{-1}, and the Si-O-Al (AlPC) or Si-O-Zr (ZrPC) bending vibration around 520 cm^{-1}. These bands support the preservation of the aluminosilicate framework and the effective formation of stable oxide pillars after pillaring. Following adsorption of AMP, several noticeable spectral changes were observed, providing direct evidence of adsorbate–adsorbent interactions. The broad O-H stretching vibration shifted slightly from approximately 3430-3440 cm^{-1} to 3420-3425 cm^{-1} with a slight change in band intensity, indicating the participation of surface hydroxyl groups in hydrogen-bond formation with AMP molecules. Simultaneously, the H-O-H bending vibration shifted from approximately 1630 cm^{-1} to 1635 cm^{-1}, accompanied by the appearance of a new absorption

band at 1655 cm^{-1}, which corresponds to the amide I (C=O stretching) vibration of adsorbed ampicillin. In addition, a distinct band developed at approximately 1540 cm^{-1}, assigned to amide II (N-H bending) vibrations, while another new band appeared around 1240 cm^{-1}, corresponding to C-O/C-N stretching vibrations of AMP. The appearance of these characteristic AMP bands suggests the effective immobilisation of antibiotic molecules onto the pillared clay surfaces. Importantly, the framework vibrations of Si-O stretching (1030 cm^{-1}) and Si-O-Al/Si-O-Zr bending (approx. 520 cm^{-1}) remained largely unchanged after adsorption, although slight reductions in intensity were observed. The absence of significant shifts in these structural bands indicates that the aluminosilicate framework and the oxide pillars remained structurally stable throughout the adsorption process. This observation suggests that adsorption primarily occurred through surface interactions rather than structural transformation or degradation of the pillared clays. The slight shift of hydroxyl-related bands together with the emergence of characteristic ampicillin functional groups suggests that hydrogen bonding plays a major role during adsorption. Surface silanol (Si-OH) groups and hydroxylated Al-OH/Zr-OH species can interact with the amino ($-NH_2$), hydroxyl (-OH), carboxyl ($-COOH/-COO^-$), and β-lactam carbonyl groups of AMP through multiple hydrogen-bonding configurations. Moreover, the presence of hydroxylated aluminium and zirconium oxide pillars provides Lewis acidic centres capable of interacting with the electron-rich oxygen atoms of carboxylate and carbonyl groups in AMP through weak Lewis acid-base interactions. These interactions are consistent with the slight modifications observed in the hydroxyl and framework vibrations without the formation of new inorganic bonds.

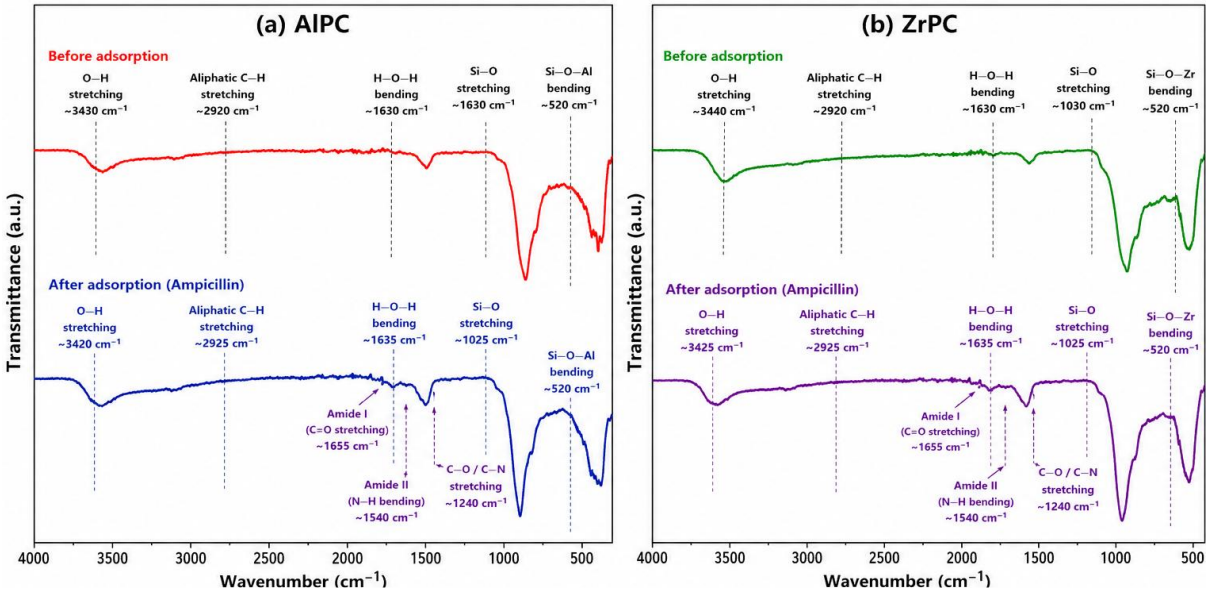


Figure 12: FTIR spectra of a) AlPC and b) ZrPC before and after adsorption of AMP, showing characteristic shifts and appearance of bands corresponding to AMP functional groups, confirming successful adsorption.

The FTIR observations are in agreement with the XPS analysis, where the appearance of the N 1s signal and slight shifts in the O 1s, Al 2p, and Zr 3d spectra indicate changes in the local chemical environment after adsorption. Likewise, the FTIR results complement the BET and XRD analyses, indicates the substantial increases in surface area, microporosity, and interlayer spacing following pillaring, thereby facilitating pore filling and molecular confinement of AMP within the expanded clay galleries. Furthermore, the pH-dependent adsorption behaviour and pH_{pzc} results indicate that electrostatic attraction between deprotonated AMP species and positively polarised hydroxylated metal sites also contributes to adsorption under favourable pH conditions.

The thermodynamic results revealed negative values of $\Delta H°$, indicating that adsorption is exothermic. The relatively low magnitude of the enthalpy changes suggests that adsorption is predominantly physical in nature. Therefore, electrostatic interactions, hydrogen bonding, and pore-filling effects are considered to be the major contributors to adsorption, whereas Lewis

acid-base interactions may provide an additional contribution to the overall adsorption mechanism. Although both AlPC and ZrPC exhibit similar adsorption pathways, AlPC shows better adsorption capacity than ZrPC. This behaviour is primarily attributed to its larger specific surface area, greater micropore volume, and slightly larger interlayer spacing, which provide improved accessibility of adsorption sites and facilitate molecular diffusion within the porous framework. The adsorption of AMP is proposed to involve a synergistic process dominated by electrostatic interactions, hydrogen bonding, and pore-filling effects, with additional contributions from Lewis acid-base interactions. The structural modifications appear to contribute substantially to enhancing adsorption performance by increasing surface area, developing hierarchical porosity, and improving accessibility to active sites.

3.4.Economic cost analysis and environmental suitability

Valuation of the economic features of the developed adsorbent materials is a much more important aspect in defining their suitability for real-world implementation. The cost evaluation is performed to scrutinise the possibility of producing AlPC and ZrPC, considering production cost, raw precursor bentonite (BT), chemical inputs, energy consumption during processing, and ancillary laboratory operations [51]. The starting material is obtained from a local supplier in Wroclaw city, Poland, at 8 Polish złoty per kilogram (equivalent to 1.89 € kg^{-1}). Transportation costs are considered insignificant, as material handling and travel were covered through routine public transport usage. Further, owing to the simplicity of the synthesis process and the limited utility of specialised or automated equipment, labour-related expenses are also regarded as negligible and therefore excluded from the cost calculation. Therefore, the preparation cost is determined using the following expression: [51,52]:

$$\text{Preparation cost} = BC + CGC + SHC + CC + OU + WC$$

BC represents raw bentonite clay in the form of lumps, *CGC* represents the crushing and grinding cost, *SHC* is the stirring & heating cost, *CC* is the calcination cost, *OU* is the other utility cost, and *WC* is the washing cost. The calculated cost of preparation of both the adsorbent materials is summarised in **Table 4**.

Table 4: Cost assessment of preparation of 1 kg of AlPC and ZrPC

AlPC	**€ per Kg**	**ZrPC**	**€ per Kg**
BC	1.89	BC	1.89
CGC	0	CGC	0
SHC*	0.02	SHC*	0.02
CC	0.18	CC	0.12
OU	3.50	OU	2.90
WC	0.3	WC	0.2
Total cost	**5.89**	**Total**	**5.13**

***** *Activity cost = Time (h) ∗ Equipment Power (kW) ∗ electricity cost in Poland*

For instance, BC lumps were manually crushed and ground using a mortar and pestle, and washing costs are considered negligible due to the availability of deionised water. The total expenditure is associated with the cost of raw materials, chemicals used, drying, stirring & heating at different levels, and calcination (energy consumed in the furnace). The cost valued to AlPC preparation is 5.89 € per Kg and for 1.0 g preparation is 0.0058 €. Whereas for ZrPC is 5.13 € per Kg and 0.00513 € for 1.0 g of production. While starting material BT is used as an adsorbent with negligible preparation cost, which only includes purchasing cost, *i.e.,* 1.89 € per Kg. Whereas the comparison of adsorption efficiency with others is presented in Table 5.

764 **Table 5. Comparison of prepared adsorbents with AlPC and ZrPC for the removal of**

765 **AMP**

S.No.	Adsorbents	Adsorption capacity, mg. g^{-1}	References
1	CB (Biochar)	18.97	[53]
2	Iron and cerium nanoparticles (C-Fe/Ce)	27.61	
3	Manganese dioxide/MMT	45	[54]
4	Organobentonite	46.6	[55]
5	Silver nanoparticles were incorporated with chitosan	49.5	[56]
6	Integrated Biochar	53.81	[57]
7	ZrPC	59.17	Present study
8	Activated carbon modified with HNO_3 oxidation	59.8	[58]
9	Bentonite- chitosan composite	66	[59]
10	AlPC	73.67	Present study
11	Activated carbon	90	[58]
12	Polydopamine/zirconium(iv) iodate	100	[60]
13	Activated carbon (AAC) modified through thermal treatment	140.9	[58]

14	Granular activated carbon (GAC)	204	[61]

766

767 The prepared adsorbent materials, AlPC and ZrPC, illustrate substantial environmental
768 suitability, which is consistent with circular bioeconomy principles and sustainable
769 management. The utility of abundant bentonite clay at low cost or collected from nature reveals
770 resource efficiency and no-cost investment in the collection of raw material. The exhaustion of
771 a limited amount of chemicals in synthesis helps to potentially reduce the carbon footprint
772 compared to the production of other adsorbents. Additionally, calcination of both the adsorbent
773 materials under 773 K and maximum achieved adsorption capacity for AlPC (73.67 mg. g^{-1})
774 and ZrPC (59.17 mg. g^{-1}), under basic conditions (> pH 7), may be considered as competitive
775 adsorbents (Table 3). When compared with previously reported adsorbents for the removal of
776 AMP, AlPC and ZrPC exhibit competitive adsorption efficiency. Table 5 summarises the
777 comparison of the adsorption efficiency of AlPC and ZrPC with other adsorbents as reported
778 earlier. Many conventional adsorbents, such as activated carbons, biochars, and polymer-based
779 materials, often require complex synthesis routes, a much longer process, higher energy input,
780 or exclusive precursors, which cause increased production costs. In addition, such adsorbents
781 have limited regeneration efficiency or rapid performance decline after repeated use.
782 Meanwhile, AlPC and ZrPC maintained stable adsorption efficiency over multiple adsorption-
783 desorption cycles (>3) and are effectively regenerated using 0.1 M NaOH. Hence, it is
784 important to highlight that the aspect of reusing these adsorbents appeals to their economic
785 attractiveness and limits waste generation, attracting the concept of environmental
786 sustainability. Moreover, the potential for localised production using readily available materials
787 may further reduce transportation-related emissions and operational costs.

788 **4. Performance of adsorbents for real wastewater**

The practical applicability of the developed pillared clays was evaluated using hospital wastewater collected from Doon Hospital. Hospital effluents represent a complex aqueous matrix containing many pharmaceutical residues, dissolved organic matter, suspended solids, and various inorganic ions that can significantly influence adsorption behaviour. The wastewater used in this study exhibited a near-neutral pH (7.2), chemical oxygen demand (COD) of 420 mg. L^{-1}, total dissolved solids (TDS) of 780 mg. L^{-1}, and contained competing ionic species, including chloride and ammonium ions. The adsorption performance of AlPC and ZrPC toward AMP was investigated under the same operating conditions employed for synthetic aqueous solutions. As expected, the adsorption efficiencies obtained in the real wastewater matrix were lower than those observed for the synthetic systems due to the presence of challenging constituents. AlPC attain an AMP removal efficiency of 77.4%, corresponding to an adsorption capacity of 57.2 mg. g^{-1}, whereas ZrPC exhibits a removal efficiency of 69.3% with an adsorption capacity of 44.8 mg. g^{-1}. Relative to the adsorption capacities obtained in synthetic solutions, AlPC and ZrPC retained approximately 77.6% and 75.7% of their maximum adsorption capacities, respectively, demonstrating substantial adsorption performance under realistic operating conditions. The observed reduction in adsorption efficiency can be attributed to electrostatic screening effects caused by dissolved inorganic ions, which weaken the interactions between AMP molecules and the adsorbent surface. In addition, natural organic matter and other dissolved contaminants compete for active adsorption sites and may partially block the micro - mesoporous structure of the adsorbents, thereby reducing the accessibility of adsorption sites. Such matrix effects are commonly reported in the treatment of real wastewaters and represent a major challenge for adsorption-based technologies. Despite these competitive effects, both pillared clays maintained considerable adsorption capacities, highlighting their robustness in complex wastewater

environments. Among the investigated materials, AlPC exhibited superior performance owing to its larger specific surface area, higher micropore volume, and expanded interlayer spacing generated during the pillaring process. These structural characteristics facilitate mass transfer and provide enhanced accessibility to adsorption sites even in the presence of competing species. Furthermore, the hydroxylated aluminium oxide pillars may contribute additional interaction sites for AMP adsorption through hydrogen bonding and Lewis acid - base interactions. The regeneration performance of the adsorbents was also evaluated under repeated adsorption - desorption conditions. AlPC retained approximately 80% of its initial adsorption efficiency after three consecutive regeneration cycles, whereas ZrPC retained approximately 72%, indicating reasonable operational stability and structural integrity. The gradual decline in performance is likely associated with partial pore blockage and irreversible adsorption of organic constituents present in the wastewater matrix. Nevertheless, both materials demonstrated satisfactory regeneration behaviour, shows their suitability for repeated application. Although the adsorption performance declines in complex wastewater matrices relative to synthetic solutions, the developed pillared clays remain effective for AMP removal. The combination of high adsorption capacity, favourable regeneration behaviour, low preparation cost, and stable performance under realistic conditions highlights their potential for practical wastewater treatment applications. Among the investigated materials, AlPC emerged as a promising adsorbent due to its better adsorption efficiency and regeneration stability.

5. Conclusion

The present study investigates the synthesis of AlPC- and ZrPC pillared bentonites via a microwave-sonochemical hybrid fusion strategy, ensuring enhanced control over the physicochemical properties of pillared clay systems. The combined effects of microwave-assisted hydrolysis and sonochemical dispersion significantly improved the surface area, their

porosity, and interlayer accessibility, leading towards higher/ better adsorption performance as compared to pristine bentonite. Pillaring with Al^{3+} and Zr^{4+} generated abundant Lewis-acidic sites, establishing a clear structure - performance relationship leading to adsorption behaviour. Mechanistic analysis exposes that adsorption is driven by a synergistic interplay of electrostatic interactions, surface complexation with Lewis-acidic centres, and pore confinement within the hierarchical micro - mesoporous framework. The adsorption performance of AlPC (73.67 $mg.g^{-1}$) compared to ZrPC highlights the critical role of pillar chemistry and dispersion efficiency in optimising the adsorption capacity. The thermodynamic and kinetic evaluation supports a spontaneous, diffusion - assisted process with mixed physisorption - chemisorption characteristics. The materials further exhibit stable reusability with high desorption efficiency under mild regeneration conditions, supporting their operational feasibility. Their application for real hospital wastewater matrix of effluents from Doon Hospital shows removal efficiencies of 81.2% and 74.6%, respectively. Although the current cost assessment is preliminary, the use of abundant natural clay precursors combined with a potentially time-efficient hybrid synthesis route suggests strong prospects for scale-up and cost reduction. This work establishes the hybrid - assisted pillaring as a promising trail for designing next - generation adsorbents for emerging contaminant removal.

Limitations of the Study

Although the developed adsorbents display promising performance and were evaluated using representative hospital wastewater, the present study has several limitations. First, the adsorption experiments were conducted under laboratory-scale batch conditions, which may not fully represent the hydrodynamic and operational conditions encountered in continuous-flow or full-scale wastewater treatment systems. Second, the adsorption performance was primarily evaluated for ampicillin; therefore, the applicability of the developed adsorbents

toward other pharmaceuticals, emerging contaminants, or complex contaminant mixtures requires further investigation. In addition, the influence of competing ions and natural organic matter present in different wastewater matrices warrants more comprehensive evaluation. Furthermore, the regeneration study was limited to three adsorption-desorption cycles. Although the pillared clays retained satisfactory adsorption performance over the investigated cycles, additional long-term studies are required to assess their structural stability, adsorption efficiency, and regeneration performance under extended operational conditions. Finally, the techno-economic assessment presented in this work is preliminary and based on laboratory-scale production. It does not consider pilot-scale operation, process optimisation, life-cycle environmental impacts, or detailed economic analyses associated with industrial implementation. Therefore, further pilot-scale investigations and comprehensive economic and environmental assessments are necessary to establish the practical feasibility of large-scale application of the developed adsorbents.

Future Perspectives

Future research should focus on evaluating the performance of the developed pillared clays under continuous-flow conditions to better simulate practical wastewater treatment processes. Fixed-bed column studies are recommended to investigate breakthrough behaviour, adsorption dynamics, and long-term operational stability under realistic hydraulic conditions. In addition, the adsorption performance should be assessed in wastewater containing multiple pharmaceuticals, emerging contaminants, competing inorganic ions, and natural organic matter to better understand the selectivity and robustness of the adsorbents in complex environmental matrices. Further investigations involving advanced computational approaches, such as density functional theory (DFT) calculations and molecular dynamics simulations, would provide molecular-level insights into the interactions between adsorbates and the pillared clay surfaces,

thereby complementing the experimental findings and improving the understanding of the adsorption mechanism. Expanding the study to include a broader range of antibiotics and other emerging contaminants would help evaluate the versatility and applicability of the developed adsorbents across different classes of pollutants. Finally, pilot-scale investigations, together with comprehensive techno-economic analyses and life-cycle assessments, are recommended to assess the environmental sustainability, economic feasibility, and practical potential of large-scale implementation.

Funding Declaration

This work is also carried out in the International Exchange of Doctoral Students as part of the project: International Interdisciplinary Doctoral School- at the HEART of Bio-Based University, financed by the National Agency for Academic Exchange under the STER programme to Wroclaw University of Environmental and Life Sciences (UPWr), Wroclaw, Poland and Doctoral student grant at the UPWr (Agreement no. N020/0025/24).

Data availability

The findings of this study are presented in this article. Additional data, including the raw experimental data generated and analysed during the current study, are available from the corresponding author upon reasonable request.

Credit Author Statement

Prashant Pandey: Conceptualisation, Investigation, Formal analysis, Data curation, Funding acquisition and Writing original draft.

Manisha Dhiman: Methodology, Formal Analysis, Supervision, Visualisation and Writing - review & editing.

Amit Pokhriyal: Conceptualisation, Investigation, Formal analysis, Funding acquisition, Data curation and Writing original draft.

Chinenye Adaobi Igwegbe: Supervision, Visualisation and Writing - review & editing

Andrzej Białowiec: Project administration, Methodology, Formal Analysis, Supervision, Visualisation, Funding acquisition and Writing - review & editing.

Lukasz Bobak: Formal Analysis, Visualisation and Instrumentation.

Declaration of Competing Interest

The authors declare that they have no known competing financial interests or personal relationships that could have appeared to influence the work reported in this paper.

Acknowledgments

This work is also carried out in the International Exchange of Doctoral Students as part of the project: International Interdisciplinary Doctoral School- at the HEART of Bio-Based University, financed by the National Agency for Academic Exchange under the STER programme to Wroclaw University of Environmental and Life Sciences (UPWr), Wroclaw, Poland and Doctoral student grant at the UPWr (Agreement no. N020/0025/24). The authors would like to acknowledge all the members of Wroclaw University of Environmental and Life Sciences, Wroclaw, Poland, for their support at any part of the study. The article is part of a Ph.D. dissertation titled "Development of Nature-Based Adsorbent Materials for Adsorption of Antibiotics from Wastewater", prepared during the Doctoral School at the Wroclaw University of Environmental and Life Sciences, Poland.

References

1. Caneschi, A., Bardhi, A., Barbarossa, A. & Zaghini, A. The Use of Antibiotics and Antimicrobial Resistance in Veterinary Medicine, a Complex Phenomenon: A Narrative Review. *Antibiotics* **12**, 487 (2023).
2. Papatsiros, V. G. *et al.* Alternatives to antibiotics for farm animals. *CABI Rev.* 1–15 (2014) doi:10.1079/PAVSNNR20138032.
3. Benedetti, M. S. *et al.* Drug metabolism and pharmacokinetics. *Drug Metab. Rev.* **41**, 344–390 (2009).

4. Ferrara, F. *et al.* Antibacterial agents and the fight against antibiotic resistance: A real-world evidence analysis of consumption and spending by an Italian healthcare company. *Ann. Pharm. Fr.* **82**, 545–552 (2024).
5. Wilke, M. S., Lovering, A. L. & Strynadka, N. C. β-Lactam antibiotic resistance: a current structural perspective. *Curr. Opin. Microbiol.* **8**, 525–533 (2005).
6. L., R. & V., S. Penicillin G Acylase: A Multifunctional Catalyst with Broad Implications in Pharmaceutical Science and Industrial Applications. *Lett. Drug Des. Discov.* **22**, (2025).
7. Ma, Q. *et al.* Elimination of antimicrobial resistance in reclaimed water by UV/NaClO: Simultaneous removal of ampicillin, blaNDM-1-carrying super-resistant bacteria and blaNDM-1 genes. *J. Water Process Eng.* **71**, 107277 (2025).
8. Murugesan, V. *et al.* Fabrication and characterization of hydroxyapatite substituted with Mg2+, Sr2+, and ampicillin for bone and antibacterial applications. *Mater. Sci. Eng. B* **316**, 118131 (2025).
9. Burke, V. *et al.* Occurrence of Antibiotics in Surface and Groundwater of a Drinking Water Catchment Area in Germany. *Water Environ. Res.* **88**, 652–659 (2016).
10. Watkinson, A. J., Murby, E. J., Kolpin, D. W. & Costanzo, S. D. The occurrence of antibiotics in an urban watershed: From wastewater to drinking water. *Sci. Total Environ.* **407**, 2711–2723 (2009).
11. Yi, C. *et al.* Distribution and risk characteristics of antibiotics in China surface water from 2013 to 2024. *Chemosphere* **375**, 144197 (2025).
12. Sério, J., Marques, A. P., Huertas, R., Crespo, J. G. & Pereira, V. J. Occurrence and Treatment of Antibiotic-Resistant Bacteria Present in Surface Water. *Membranes* **13**, 425 (2023).
13. Kulkarni, P. *et al.* Antibiotic Concentrations Decrease during Wastewater Treatment but Persist at Low Levels in Reclaimed Water. *Int. J. Environ. Res. Public. Health* **14**, 668 (2017).
14. De Carvalho, C. B. *et al.* Degradation of ampicillin by combined process: Adsorption and Fenton reaction. *Environ. Technol. Innov.* **26**, 102365 (2022).

15. Del Vecchio, P., Haro, N. K., Souza, F. S., Marcílio, N. R. & Féris, L. A. Ampicillin removal by adsorption onto activated carbon: kinetics, equilibrium and thermodynamics. *Water Sci. Technol.* **79**, 2013–2021 (2019).
16. Nairi, V., Medda, L., Monduzzi, M. & Salis, A. Adsorption and release of ampicillin antibiotic from ordered mesoporous silica. *J. Colloid Interface Sci.* **497**, 217–225 (2017).
17. Thakur, B. *et al.* Designing of bentonite based nanocomposite hydrogel for the adsorptive removal and controlled release of ampicillin. *J. Mol. Liq.* **319**, 114166 (2020).
18. Ahile, U. *et al.* Preparation, Characterization and Application of Rice Husk Adsorbent in the Removal of Ampicillin from Aqueous Solution. (2019).
19. Rahardjo, A. K., Susanto, M. J. J., Kurniawan, A., Indraswati, N. & Ismadji, S. Modified Ponorogo bentonite for the removal of ampicillin from wastewater. *J. Hazard. Mater.* **190**, 1001–1008 (2011).
20. Rahardjo, A. K., Susanto, M. J. J., Kurniawan, A., Indraswati, N. & Ismadji, S. Modified Ponorogo bentonite for the removal of ampicillin from wastewater. *J. Hazard. Mater.* **190**, 1001–1008 (2011).
21. Thakur, B. *et al.* Designing of bentonite based nanocomposite hydrogel for the adsorptive removal and controlled release of ampicillin. *J. Mol. Liq.* **319**, 114166 (2020).
22. Gil, A., Gandía, L. M. & Vicente, M. A. Recent Advances in the Synthesis and Catalytic Applications of Pillared Clays. *Catal. Rev.* **42**, 145–212 (2000).
23. Pandey, P. & Saini, V. K. Pillared interlayered clays: sustainable materials for pollution abatement. *Environ. Chem. Lett.* **17**, 721–727 (2019).
24. Gil, A., Gandía, L. M. & Vicente, M. A. Recent Advances in the Synthesis and Catalytic Applications of Pillared Clays. *Catal. Rev.* **42**, 145–212 (2000).
25. Jeirani, Z., Niu, C. H. & Soltan, J. Adsorption of emerging pollutants on activated carbon. *Rev. Chem. Eng.* **33**, 491–522 (2017).

26. Sellaoui, L. *et al.* Adsorption of emerging pollutants on lignin-based activated carbon: Analysis of adsorption mechanism via characterization, kinetics and equilibrium studies. *Chem. Eng. J.* **452**, 139399 (2023).
27. Langmuir, I. The Evaporation, Condensation and Reflection of Molecules and the Mechanism of Adsorption. *Phys. Rev.* **8**, 149–176 (1916).
28. Freundlich, H. & Losev, G. Über die Adsorption der Farbstoffe durch Kohle und Fasern. *Z. Für Phys. Chem.* **59U**, 284–312 (1907).
29. Nasseh, N., Barikbin, B., Taghavi, L. & Nasseri, M. A. Adsorption of metronidazole antibiotic using a new magnetic nanocomposite from simulated wastewater (isotherm, kinetic and thermodynamic studies). *Compos. Part B Eng.* **159**, 146–156 (2019).
30. Khan, A. R., Al-Bahri, T. A. & Al-Haddad, A. Adsorption of phenol based organic pollutants on activated carbon from multi-component dilute aqueous solutions. *Water Res.* **31**, 2102–2112 (1997).
31. Sing, K. S. W. & Williams, R. T. Physisorption Hysteresis Loops and the Characterization of Nanoporous Materials. *Adsorpt. Sci. Technol.* **22**, 773–782 (2004).
32. Gil, A., Guiu, G., Grange, P. & Montes, M. Preparation and Characterization of Microporosity and Acidity of Silica-Alumina Pillared Clays. *J. Phys. Chem.* **99**, 301–312 (1995).
33. Draoui, K., Denoyel, R., Chgoura, M. & Rouquerol, J. Adsorption of Paraquat on minerals: A thermodynamic study. *J. Therm. Anal. Calorim.* **58**, 597–606 (1999).
34. Sing, K. S. & Williams, R. T. Physisorption hysteresis loops and the characterization of nanoporous materials. *Adsorpt. Sci. Technol.* **22**, 773–782 (2004).
35. Zhu, J., Zhu, L., Zhu, R., Tian, S. & Li, J. Surface microtopography of surfactant modified montmorillonite. *Appl. Clay Sci.* **45**, 70–75 (2009).

36. Manohar, D. M., Noeline, B. F. & Anirudhan, T. S. Adsorption performance of Al-pillared bentonite clay for the removal of cobalt(II) from aqueous phase. *Appl. Clay Sci.* **31**, 194–206 (2006).
37. Li, K. *et al.* Fe-, Ti-, Zr- and Al-pillared clays for efficient catalytic pyrolysis of mixed plastics. *Chem. Eng. J.* **317**, 800–809 (2017).
38. Bergaya, F. & Lagaly, G. Chapter 1 General Introduction: Clays, Clay Minerals, and Clay Science. in *Developments in Clay Science* vol. 1 1–18 (Elsevier, 2006).
39. Chauhan, T. *et al.* Synthesis, characterization, and challenges faced during the preparation of zirconium pillared clays. *Arab. J. Chem.* **15**, 103706 (2022).
40. Chauhan, M., Saini, V. K. & Suthar, S. Removal of pharmaceuticals and personal care products (PPCPs) from water by adsorption on aluminum pillared clay. *J. Porous Mater.* **27**, 383–393 (2020).
41. Tomul, F. & Balci, S. Characterization of Al, Cr-pillared clays and CO oxidation. *Appl. Clay Sci.* **43**, 13–20 (2009).
42. Chauhan, T. *et al.* Synthesis, characterization, and challenges faced during the preparation of zirconium pillared clays. *Arab. J. Chem.* **15**, 103706 (2022).
43. Neris, A. M., Ferreira, J. M., Fonseca, M. G. & Dos Santos, I. M. G. Undoped tetragonal ZrO2 obtained by the Pechini method: thermal evaluation of tetragonal–monoclinic phase transition and application as catalyst for biodiesel synthesis. *J. Therm. Anal. Calorim.* **143**, 3307–3316 (2021).
44. Alfred, M. O. *et al.* Solar-active clay-TiO2 nanocomposites prepared via biomass assisted synthesis: Efficient removal of ampicillin, sulfamethoxazole and artemether from water. *Chem. Eng. J.* **398**, 125544 (2020).
45. Weng, X., Cai, W., Lan, R., Sun, Q. & Chen, Z. Simultaneous removal of amoxicillin, ampicillin and penicillin by clay supported Fe/Ni bimetallic nanoparticles. *Environ. Pollut.* **236**, 562–569 (2018).

46. Gudla, V. C. *et al.* High frequency anodising of aluminium–TiO2 surface composites: Anodising behaviour and optical appearance. *Surf. Coat. Technol.* **277**, 67–73 (2015).
47. Ahmed, M. B., Zhou, J. L., Ngo, H. H. & Guo, W. Adsorptive removal of antibiotics from water and wastewater: Progress and challenges. *Sci. Total Environ.* **532**, 112–126 (2015).
48. Islam, Md. R., Wang, Q., Sharmin, S. & Enyoh, C. E. Adsorption of Ibuprofen from Water Using Banana Peel Biochar: Experimental Investigation and Machine Learning Algorithms. *Water* **16**, 3469 (2024).
49. Roca Jalil, M., Baschini, M. & Sapag, K. Removal of Ciprofloxacin from Aqueous Solutions Using Pillared Clays. *Materials* **10**, 1345 (2017).
50. Pandey, P., Shankar, A., Biney, M. & Saini, V. K. Enhancement in amoxicillin adsorption and regeneration properties of SBA-15 after surface modification with polyaniline. *Colloid Interface Sci. Commun.* **43**, 100432 (2021).
51. Al-Hazeef, M. S. *et al.* Valorizing date palm spikelets into activated carbon-derived composite for methyl orange adsorption: advancing circular bioeconomy in wastewater treatment—a comprehensive study on its equilibrium, kinetics, thermodynamics, and mechanisms. *Environ. Sci. Pollut. Res.* **31**, 50493–50512 (2024).
52. Syafiuddin, A. *et al.* Removal of silver nanoparticles from water environment: experimental, mathematical formulation, and cost analysis. *Water. Air. Soil Pollut.* **230**, 102 (2019).
53. Gómez-Vilchis, J., García-Rosales, G., Longoria-Gándara, L., Pérez-Gómez, E. & Castilleros, D. Obtention of biochar-Fe/Ce using Punica granatum with high adsorption of ampicillin capacity. *Heliyon* **8**, (2022).
54. Valovicova, V. *et al.* Removal of amoxicillin and ampicillin using manganese dioxide/montmorillonite composite. *J. Chem. Technol. Biotechnol.* **98**, 197–203 (2023).
55. Yeo, J. Y. J., Aqsha, A., Ismadji, S. & Sunarso, J. Adsorption kinetics of amoxicillin, ampicillin, and doripenem on organobentonite. in vol. 3073 070013 (AIP Publishing LLC, 2024).

56. Mahmodi sheikh sarmast, Z., Sedaghat, S., Derakhshi, P. & Aberoomand Azar, P. Efficient removal of ampicillin from aqueous media using silver nanoparticles decorated with magnetic-chitosan: optimization by central composite design. *Chem. Pap.* **78**, 189–205 (2024).
57. Yu, J. *et al.* Preparation and characterization of biochar from four different solid wastes and its ampicillin adsorption performance. *Environ. Geochem. Health* **46**, 440 (2024).
58. Li, X., Zhang, N. & Yang, L. Adsorption of ampicillin sodium on activated carbons with different surface chemistries. in *IOP Conference Series: Earth and Environmental Science* vol. 467 012184 (IOP Publishing, 2020).
59. Bouaziz, N. *et al.* Adsorption of antibiotics by bentonite-chitosan composite: Phenomenological modeling and physical investigation of the adsorption process. *Int. J. Biol. Macromol.* **242**, 125156 (2023).
60. Rahman, N. & Varshney, P. Assessment of ampicillin removal efficiency from aqueous solution by polydopamine/zirconium (iv) iodate: optimization by response surface methodology. *RSC Adv.* **10**, 20322–20337 (2020).
61. Chia, R. Y. H. Removal of ampicillin and ciprofloxacin by GAC adsorption. (2018).